# Deciphering the metamorphic evolution of the Pulo do Lobo metasedimentary domain (SW Iberian Variscides)

Irene Pérez-Cáceres[1,2], David Jesús Martínez Poyatos[1], Olivier Vidal[3], Olivier Beyssac[4], Fernando Nieto[5], José Fernando Simancas[1], Antonio Azor[1] and Franck Bourdelle[6]

1 Departamento de Geodinámica, Facultad de Ciencias, Universidad de Granada, Campus de Fuentenueva s/n, 18071 Granada, Spain.

2 Instituto de Ciencias de la Tierra Jaume Almera ICTJA-CSIC, C/Lluís Solé i Sabarís s/n, 08028, Barcelona, Spain.

3 Institut de Sciences de la Terre (ISTerre), CNRS-University of Grenoble 1, 1381 rue de la Piscine, 38041 Grenoble, France.

4 Institut de Physique des Matériaux et de Cosmochimie (IMPMC), CNRS-Sorbonne Université, Case Courrier 115, 4 place Jussieu, 75005 Paris, France.

5 Departamento de Mineralogía y Petrología, IACT, Facultad de Ciencias, Universidad de Granada-CSIC, Campus de Fuentenueva s/n, 18071 Granada, Spain.

6 Laboratoire Génie Civil et géo-Environnement (LGCgE), Université de Lille, Bât. SN5, Cité Scientifique, 59655 Villeneuve d'Ascq, France.

Correspondence to: Irene Pérez-Cáceres (perezcaceres@ugr.es)

## Abstract

The Pulo do Lobo domain is one of the units related to the orogenic suture between the Ossa-Morena and the South Portuguese zones in the SW Iberian Variscides. This metasedimentary unit has been classically interpreted as a Rheic subduction-related accretionary prism formed during the pre-Carboniferous convergence and eventual collision between the South Portuguese Zone (part of Avalonia) and the Ossa-Morena Zone (peri-Gondwanan terrane). Discrete mafic intrusions also occur in the dominant Pulo do Lobo metapelites, related to an intraorogenic Mississippian transtensional and magmatic event that had a significant thermal input. Three different approaches have been applied to the Devonian/Carboniferous phyllites and slates of the Pulo do Lobo domain in order to study their poorly known low-grade metamorphic evolution. X-Ray diffraction (XRD) was used to unravel the mineralogy and measure crystallographic parameters (illite "crystallinity" and K-white mica *b*-cell dimension). Compositional maps of selected samples were obtained from electron probe microanalysis, which allowed processing with XmapTools software, and

chlorite semi-empirical and thermodynamic geothermometry was performed. Thermometry based on Raman spectroscopy of carbonaceous material (RSCM) was used to obtain peak temperatures.

The microstructural study shows the existence of two phyllosilicate growth events at the chlorite zone, the main one ($M_1$) related to the development of a Devonian foliation $S_1$, and a minor one ($M_2$) associated with a crenulation cleavage ($S_2$) developed at middle/upper Carboniferous time. $M_1$ entered well into epizone (greenschist facies) conditions. $M_2$ conditions were at lower temperature, reaching the anchizone/epizone boundary. These data accord well with the unconformity that separates the Devonian and Carboniferous formations of the Pulo do Lobo domain. The varied results obtained by the different approaches followed, combined with microstructural analysis, are indicative of different snapshots of the metamorphic history. Thus, RSCM temperatures are higher in comparison with the other methods applied, which is interpreted as reflecting a faster reequilibration during the short-lived thermal Mississippian event. Regarding the metamorphic pressure, the data are very homogeneous: very low celadonite content (0-10 %) in muscovite (and low values of K-white mica *b*-cell dimension (8.995 Å mean value), indicating a low pressure/temperature gradient, which is unexpected in a subduction-related accretionary prism.

**Keywords**

Pulo do Lobo metapelites

Low-pressure gradient

Illite "crystallinity"

Chlorite geothermometry

Raman spectroscopy of carbonaceous material

**Highlights**

A multidisciplinary approach has been applied to study the metamorphism of the Pulo do Lobo metapelites.

Devonian metamorphism entered epizone conditions.

Carboniferous metamorphism reached the anchizone/epizone boundary.

The inferred low-pressure gradient is incompatible with a subduction-related accretionary prism.

## 1. Introduction

The knowledge of temperature and pressure conditions reached by the low-grade metasedimentary units stacked hinterlands of orogens helps to better interpret their tectonometamorphic evolution (e.g., Goffé and Velde, 1984; Franceschelli et al., 1986; Ernst, 1988; Gutiérrez-Alonso and Nieto, 1996; Frey and Robinson, 1999; Bousquet et al., 2008; Lanari et al., 2012). In this regard, the various results derived from the application of diverse geothermometric and/or geobarometric methods may also allow the identification and characterization of superposed tectonometamorphic events, thus improving the knowledge of the P-T paths and their tectonic significance (e.g., Brown, 1993; Crouzet et al., 2007; Ali, 2010; Lanari et al., 2012; Airaghi et al., 2017).

The metamorphism of the Iberian Variscides has been mostly studied on intensely metamorphosed rocks in order to characterize high-grade events and obtain the P-T-t paths of suture-related units (e.g., Gil Ibarguchi et al., 1990; Abalos et al., 1991; Escuder Viruete et al., 1994; Barbero, 1995; Arenas et al., 1997; Fonseca et al., 1999; López-Carmona et al., 2013; Martínez Catalán et al., 2014). The low- to very low-grade units have been also studied (e.g., Martínez Catalán, 1985; Bastida et al., 1986, 2002; López Munguira et al., 1991; Gutiérrez-Alonso and Nieto, 1996; Abad et al., 2001, 2002, 2003a; Martínez Poyatos et al., 2001; Nieto et al., 2005; Vázquez et al., 2007), despite the scarcity of appropriate robust methodologies to apply in these kind of rocks. Obtaining new results from the low-grade rocks of the Pulo do Lobo domain, a suture-related low-grade unit in SW Iberia, is of capital importance in order to understand its significance and tectonometamorphic evolution, that have been cause of discrepancies, and to reconstruct the overall history of the SW Iberian Variscides.

In this work, three different methodologies are applied to a number of samples of the Pulo do Lobo domain (Fig. 1): (i) X-Ray Diffraction (XRD) in order to identify minerals not easily recognizable with optical microscopy (fine-grained muscovite, paragonite, mixed-layer phyllosilicates, etc.) and obtain thermobarometric information via the measurement of crystallographic parameters (illite "crystallinity" and *b*-cell dimension); (ii) Compositional maps derived from electron probe microanalysis (EPMA), which enable the recognition of different tectonometamorphic events by combining mineral composition and microtextural features (e.g., Airaghi et al., 2017), as well as the application of geothermobarometers based on chlorite and K-white mica compositions; and (iii) Raman spectroscopy of carbonaceous material (RSCM) to estimate peak temperatures thanks to an adapted thermometric calibration. Firstly, the results obtained enables discussing the tectonometamorphic evolution of the Pulo do Lobo domain. Moreover, the comparison of the different approaches allows to know further their reliability and sensitivity to characterize different geological processes.

## 2. Geological setting

The SW Iberian Variscides resulted from the Devonian-Carboniferous left-lateral oblique collision of three different terranes: the Central Iberian Zone (CIZ), the Ossa-Morena Zone (OMZ) and the South Portuguese Zone (SPZ) (Fig. 1a). The boundaries between these terranes are considered as orogenic sutures (e.g., Quesada, 1990; Pérez-Estaún and Bea, 2004;

Pérez-Cáceres et al., 2016). Besides the dominant left-lateral shortening kinematics, SW Iberia also attests Mississippian synorogenic sedimentary basins, widespread mafic magmatism and high-temperature metamorphic areas, which altogether reveal an intraorogenic transtensional stage (Simancas et al., 2003, 2006; Pereira et al., 2012; Azor et al., 2019).

The OMZ is commonly interpreted as a continental piece that drifted from the CIZ (i.e., north Gondwana) in early Paleozoic times (Matte, 2001). The OMZ/CIZ suture (Badajoz-Córdoba Shear Zone) includes early Paleozoic amphibolites with oceanic affinity, eclogite relicts and intense high- to low-grade left-lateral shear imprint (Burg et al., 1981; Abalos et al., 1991; Azor et al., 1994; Ordóñez-Casado, 1998; López Sánchez-Vizcaíno et al., 2003; Pereira et al., 2010). Ediacaran to Carboniferous sedimentary successions with an unconformity at the base or the Lower Carboniferous characterize the OMZ. Low-grade regional metamorphism dominates the OMZ, though there are areas of high-temperature / low-pressure metamorphism associated with Early Carboniferous magmatism (e.g. Bard, 1977; Crespo-Blanc, 1991; Díaz Azpiroz et al., 2006; Pereira et al., 2009).

The SPZ is a continental piece considered as a fragment of Avalonia, and thus the OMZ/SPZ boundary is usually interpreted as the Rheic Ocean suture (Crespo-Blanc and Orozco; 1988; Eden and Andrews, 1990; Silva et al., 1990; Quesada et al., 1994; Braid et al., 2011; Pérez-Cáceres et al., 2015, 2017). This boundary is delineated by the Beja-Acebuches Amphibolites (Fig. 1b), a narrow strip of metamafic rocks that resembles a dismembered ophiolitic succession (from greenschists to metagabbros and locally ultramafic rocks) (e.g., Bard, 1977; Crespo-Blanc, 1991; Quesada et al., 1994). This unit was interpreted as a Rheic ophiolite (Munhá et al., 1986; Crespo-Blanc, 1991; Fonseca and Ribeiro, 1993; Quesada et al., 1994; Castro et al., 1996), though this idea was reconsidered based on the Mississippian age of the mafic protholits (≈340 Ma; Azor et al., 2008). At present, the Beja-Acebuches unit is better interpreted as an outstanding evidence of the early Carboniferous intraorogenic, lithospheric-scale transtensional and magmatic episode that here obscures the previous suture-related features of the OMZ/SPZ boundary (Pérez-Cáceres et al., 2015 and references therein). Nevertheless, there is also the alternative explanation that the OMZ/SPZ boundary was a protected tract of Rheic oceanic lithosphere that did not close until Carboniferous time (Murphy et al., 2016; Braid et al., 2018; Quesada et al., 2019). The rocks of the Beja-Acebuches Amphibolites were affected by a left-lateral ductile shearing that occurred at granulite to greenschist facies conditions, though amphibolite facies conditions were dominant (e.g., Quesada et al., 1994; Castro et al., 1996; Castro et al., 1999; Díaz Azpiroz et al., 2006). This metamorphism has been dated at 345-330 Ma (Dallmeyer et al., 1993; Castro et al., 1999), thus suggesting that it started very shortly after the magmatic emplacement.

North of the Beja-Acebuches Amphibolites, the allochthonous Cubito-Moura unit might be the only witness of the Rheic Ocean suture (Fonseca et al., 1999; Araújo et al., 2005; Pérez-Cáceres et al., 2015). This unit was emplaced onto the southern OMZ border (Fig. 1b) with a left-lateral top-to-the-ENE kinematics (Ponce et al., 2012). It contains Ediacaran-Lower Paleozoic metasediments and Ordovician MORB-featured mafic rocks (≈480 Ma; Pedro et al., 2010) transformed into high-pressure blueschists and eclogites at ≈370 Ma (Moita et al., 2005). The high-pressure metamorphism has also been studied by using white mica and

chlorite (and chloritoid pseudomorphs) mineral equilibria (Booth-Rea et al., 2006; Ponce et al., 2012; Rubio Pascual et al., 2013), yielding peak conditions of 1 GPa at 450 °C.

South of the Beja-Acebuches Amphibolites, low- to very low-grade successions crop out: Devonian siliciclastics, earliest Carboniferous volcano-sedimentary rocks, and a south-migrating Carboniferous flysch (e.g., Oliveira, 1990). These rocks are usually grouped into two geological domains: the Pulo do Lobo domain to the north, and the SPZ s. str. to the south (Fig. 1a, b). The deformation in the SPZ consists in a south- to southwest-vergent fold and thrust belt with decreasing strain intensity and age southwards (Oliveira, 1990; Simancas et al., 2004). The metamorphic grade also decreases southwards, from epizone to diagenesis, through the SPZ (Munhá, 1990; Abad et al., 2001). The Pulo do Lobo domain, which has been traditionally considered as a suture-related unit (see below) is the focus of this work.

### 2.1. Pulo do Lobo domain

The Pulo do Lobo domain constitutes a polydeformed structure affecting low-grade Devonian-Carboniferous sedimentary formations. These formations are, from bottom to top (Fig. 1b-c):

(i) The Pulo do Lobo formation (s. str.), which is constituted by a succession of satiny black to grey phyllites and fine-grained schists with minor intercalations of quartz sandstones (Fig. 2a). The presence of abundant segregated quartz veins (pre- to post-folding) is common. The palynological content suggests a middle Frasnian age (Pereira et al., 2018).

(ii) The Ribeira de Limas formation, which is constituted by phyllites with thin beds of quartz sandstones and arkoses (Fig. 2b). The presence of palynomorphs also suggests a middle Frasnian age for this formation (Pereira et al., 2018). The contact with the underlying Pulo do Lobo formation is gradual, with a progressive increase of sandstones and a decrease of phyllites upwards. For that reason, we will refer to the Pulo do Lobo and Ribeira de Limas formations as the lower formations of the Pulo do Lobo domain. Furthermore, these lower formations share the same structure consisting in three fold-related foliations (Fig. 2a-b; Pérez-Cáceres et al., 2015). The first foliation of the lower formations ($S_1$) is preserved inside microlithons of the second foliation ($S_2$); usually, the angle between these two foliations is high. $S_2$ is the main foliation and consists in a crenulation-dissolution cleavage that frequently appears as a milimetric- to centimetric-spaced tectonic banding. This foliation is axial-plane to north-vergent folds. The third foliation ($S_3$) is a spaced crenulation-dissolution cleavage that sometimes develops a characteristic decimetric- to metric-scale tectonic banding. $S_3$ is associated with upright to slightly south-vergent folds.

(iii) The Santa Iría formation, which is composed by alternating beds of slates and greywackes (Fig. 2c). The greywacke beds show normal grading and erosive base. Paleontological and palynostratigraphic studies suggest an Upper Famennian age for this formation (Pereira et al., 2008; 2018). However, an early Carboniferous age is much plausible, since more than 90% of the palynomorphs correspond to reworked material (Lopes et al., 2014) and the younger detrital zircon population is early Carboniferous (Braid et al., 2011; Pérez-Cáceres et al., 2017; Pereira et al., 2019). The Santa Iría formation only shows two foliations, correlative with the last two deformation phases in the lower formations. Therefore, an

unconformity between them is inferred, which also agrees with the age and flysch character of the Santa Iría formation (Pérez-Cáceres et al., 2015). $S_2$ is observed as a penetrative slaty cleavage, while $S_3$ is a disjunctive crenulation cleavage.

According to Silva et al. (1990) and Pérez-Cáceres et al. (2015), the two main foliations ($S_2$ and $S_3$) in the Pulo do Lobo domain resulted from the middle/upper Carboniferous collision between the OMZ and SPZ. On the contrary, the first foliation ($S_1$) in the Pulo do Lobo domain might have formed during the vanishing stages of Rheic Ocean subduction and/or the starting Variscan collision, probably at Late Devonian time.

The Pulo do Lobo domain contains some decimetric- to metric-scale lenticular bodies of MORB-featured metamafic rocks. At some outcrops, the mafic rocks are embbeded in a greenish detrital matrix, thus suggesting an olistostromic origin (the Peramora Olistostrome; Eden and Andrews, 1990). These rocks are tectonically imbricated with the phyllites of the Pulo do Lobo formation and hence forming a tectonic mélange (the so-called Peramora Mélange; Fig. 1b-c; Eden, 1991; Dahn et al., 2014). Based on this aspect and on the supposedly Rheic Ocean derived greenschists, the Pulo do Lobo domain has been classically interpreted as a pre-collisional subduction-related accretionary prism (Eden and Andrews, 1990; Silva et al., 1990; Eden, 1991; Braid et al., 2010; Ribeiro et al., 2010; Dahn et al., 2014; Quesada et al., 2019). However, the recently obtained Mississippian U/Pb zircon ages from the metamafic rocks (Dahn et al., 2014; Pérez-Cáceres et al., 2015) make difficult to maintain such hypothesis. More properly, they can be interpreted as mafic intrusions/extrusions in the frame of the intraorogenic transtensional magmatic event that prevailed in SW Iberia during the Mississippian. The metamafic rocks display a foliation (equivalent to the $S_2$ of the enveloping metasediments) developed at loosely constrained greenschist facies conditions. These rocks would have been imbricated with the Pulo do Lobo metasediments during the second deformation phase which caused $S_2$ (Pérez-Cáceres et al., 2015). Our multidisciplinary metamorphic study of the Pulo do Lobo metasediments provides with crucial data concerning the tectonic significance of this domain.

## 3. Samples and analytical methods

Eighteen samples were collected from well-exposed outcrops of phyllosilicate-rich detrital rocks of the Pulo do Lobo domain along two north-south transects perpendicular to the structural trend. Five samples belong to the Santa Iría formation (unconformable upper formation) and thirteen to the lower formations (Pulo do Lobo and Ribeira de Limas formations) (location of samples are in the map and cross-sections of Fig. 1b-c and the UTM coordinates in supplementary information). As a whole, the samples were selected in non-altered outcrops, far from faults and joints, and were taken as homogeneous as possible. Sampling design was intended to collect representative sites, both of the overall stratigraphic succession and along the two transects. We also aimed to characterize the unconformity between the lower and upper formations from a metamorphic point of view, since "crystallinity" aspect at first sight seems to be lower in the Santa Iría formation. Some samples from the lowermost Pulo do Lobo formation were collected not far from the metabasite lenses of the Peramora Mélange.

Samples were examined under the optical microscope and scanning electron microscope (SEM) for overall mineralogy, deformation and minerals/foliations relationships using an environmental scanning electron microscope FEI model Quanta 400, operating at 15–20 keV (Centro de Instrumentación Científica-CIC, University of Granada, Spain).

### 3.1. X-Ray diffraction

Sample preparation and analysis by XRD were done in the laboratories of the Department of Mineralogy and Petrology of the University of Granada (Spain). After washing and cleaning of patinas and oxides, samples were crushed to a <2 mm fraction. The <2 μm fractions were separated by repeated extraction of supernatant liquid after centrifugation, according to the Stokes' law. Oriented aggregates were prepared by sedimentation on glass slides of whole-rock and <2 μm fractions (the latter aims to minimize the content of detrital micas non-re-equilibrated during very low-grade metamorphism, which are generally larger than 2 μm; Moore and Reynolds, 1997). Samples were also treated with ethylene glycol (EGC) to identify illite/smectite or chlorite/smectite mixed-layers on the basis of their expansibility. Samples were analyzed using a PANalytical X'Pert Pro powder diffractometer equipped with an X'Celerator detector, CuKα radiation, operated at 45 kV and 40mA, Ni filter and 0.25° divergence slit. The resulting diffraction diagrams were examined to extract information on mineralogy based on their characteristic reflections and white mica crystal data.

The Illite "Crystallinity" index (Kübler Index; KI; Kübler, 1968) has been estimated from the measurement of the full peak-width of K-white mica at half maximum intensity (FWHM values), expressed as Δ°2θ of the Bragg angle. Preparation of samples and experimental conditions were carried out according to IGCP 294 IC Working Group recommendations (Kisch, 1991). A step increment of 0.008° 2θ and a counting time of 52 s/step were used in the diffractometer. The KI has been measured in all samples for both the 5 and 10 Å reflection peaks of K-white mica in order to identify possible effects of other overlapping phases (Nieto and Sánchez-Navas, 1994; Battaglia et al., 2004). Some XRD traces showing complex mixture of mixed-layered minerals were decomposed with the MacDiff software (Petschick, 2004). The FWHM values obtained in the laboratory (x) have been transformed to Crystallinity Index Standard (CIS) values (y) using the equation y=0.972x + 0.1096 (R2 = 0.942), obtained from the measure in our lab of the international standards of Warr and Rice (1994). Finally, they have been expressed in term of traditional KI values using the equation of Warr and Ferreiro Mählnlmann (2015; 'CIS' = 1.1523*Kübler index 'Basel lab' + 0.036). The lower and upper boundaries of the anchizone in the KI scale are 0.42 and 0.25 °2θ, respectively (Warr and Ferreiro Mählnlmann, 2015). The thermal range for the anchizone is estimated in c. 200-300 °C, though the KI cannot be considered as a true geothermometer (Frey, 1987; Kisch, 1987).

The *b*-cell parameter of white mica was obtained from the (060) reflection peak measured with quartz as internal standard on polished rock-slices cut normal to the sample main foliation (Sassi and Scolari, 1974). The *b*-cell dimension of K-white mica is often proportional to the magnitude of phengitic substitution and therefore considered as a proxy of the pressure conditions during its crystallization. Thus, Guidotti and Sassi (1986) have shown

that *b* values lower than 9.000 Å are typical of low-pressure facies conditions, while *b* values higher than 9.040 Å are related to rather high-pressure facies metamorphism. Precise measurements of the basal spacing of white mica ($d_{001}$) have also been made, using quartz from the sample itself as internal standard. $d_{001}$ is related to the paragonitic Na/K substitution (Guidotti et al., 1992), thereby approximately reflecting the temperature of white-mica formation (Guidotti et al., 1994).

### 3.2. EPMA-derived X-Ray compositional maps and chlorite thermometry

From all of the collected samples, we selected those with the larger phyllosilicate grain-size for electron probe microanalysis (EPMA). Thus, three carbon-coated polished thin-sections were studied. The selected samples (PLB-84, PLB-88 and PLB-93) belong to the lower formations of the Pulo do Lobo domain (Fig. 2d-e). The Santa Iría samples could not be studied due to the tiny grain size of the slaty minerals (commonly less than 3 μm).

Compositional maps and accurate spot analyses were performed on a JEOL JXA-8230 EPMA at the Institut des Sciences de la Terre (ISTerre) in Grenoble (France), according to the analytical procedure proposed by de Andrade et al. (2006) and Lanari et al. (2014a). The data acquisition was made in wavelength dispersive spectrometry mode (WDS). Ten elements (Si, Ca, Al, K, Mn, Na, P, Ti, Fe and Mg) were analyzed using five WD spectrometers: TAP crystal for Si and Al, PETL for Ti and P, TAPH for Na and Mg, PETH for K and Ca, and LIFH for Mn and Fe. The standardization was made by using certified natural minerals and synthetic oxides: wollastonite (Si, Ca), corundum (Al), orthoclase (K), rhodonite (Mn), albite (Na), apatite (P), rutile (Ti), hematite (Fe), and periclase (Mg). X-Ray maps were obtained by adding successive adjacent profiles. Beam current of 100 nA and beam size spot (focused) were used. The step (pixel) size was 1 μm and dwell time was 200-300 msec per pixel. Spot analyses were obtained along the profiles within the mapping at 15 kV accelerating voltage, 12 nA beam current and 2 μm beam size spot (focused). The on-peak counting time was 30 sec for each element and 30 sec for two background measurements at both sides of the peak. ZAF correction procedure was applied. The internal standards were orthoclase and/or chromium-augite (Jarosewich et al., 1980), which were run (3 points on each standard) after each profile in order to monitor instrumental drift and estimate analytical accuracy. Drift correction was made, if necessary, using the corresponding regression equation.

The WDS X-Ray maps were then processed with XMapTools (http://www.xmaptools.com), a MATLAB©-based graphical user interface program to process the chemical maps, link them to thermobarometric models and estimate the pressure-temperature conditions of crystallization of minerals in metamorphic rocks (Lanari et al., 2014a). The compositional maps were standardized with the spot analyses measured along the profiles and mineral compositions were plotted into binary and ternary diagrams using the interface modules *Chem2D and Triplot3*D. Chemical maps of amount of tetrahedral aluminum ($Al^{IV}$) of chlorites were acquired, because is at the base of many empirical chlorite thermometers (e.g. Cathelineau and Nieva, 1985; Cathelineau, 1988). The temperature conditions were estimated for each chlorite pixel of the maps using the chlorite thermometer

of Lanari et al. (2014b), as well as the approaches of Vidal et al. (2006) and Bourdelle et al. (2013), which are summarized in the supplementary information.

In addition to the above mentioned compositional maps, white micas from seven carbon-coated thin sections of the lower formations of the Pulo do Lobo domain were analyzed before with a Jeol WDS four-spectrometer microprobe (JXA-8200 Superprobe) at the University of Huelva (Spain). A combination of silicates and oxides were used for calibration: standards used were wollastonite (Si and Ca), potassium feldspar (Al, K and Na), forsferite (Mg) and fayalite (Fe). Single point analyses were obtained with 20 nA probe current, 1-5 μm spot size and 15 kV of acceleration voltage, with 5 s counting times.

### 3.3. Raman Spectroscopy of carbonaceous material

Raman Spectroscopy of Carbonaceous Material (RSCM), is based on the observation that sedimentary carbonaceous material (CM) is progressively transformed into graphite at increasing temperature. Because of the irreversible character of graphitization, CM structure is not sensitive to the retrograde path during exhumation of rocks, but only depends on the maximum temperature reached during metamorphism (Beyssac et al., 2002a). Temperature can be determined in the range 330-650°C with a calibration-attached accuracy of ± 50 °C due to uncertainties on petrologic data used for the calibration. Relative uncertainties on temperature are, however, much smaller (around 10-15 °C; Beyssac et al., 2004). For temperature below 330 °C, Lahfid et al. (2010) performed a systematic study of the evolution of the Raman spectrum of CM in low-grade metamorphic rocks in the Glarus Alps (Switzerland). They showed that the Raman spectrum of CM is slightly different from the spectrum observed at higher temperature and they established a quantitative correlation between the degree of ordering of CM and temperature.

In this work, twelve representative thin-sections previously examined by optical microscopy were selected. From them, ten samples were finally analyzed (according to their larger CM grain-size and content): eight samples belong to the lower formations (Pulo do Lobo and Ribeira de Limas formations), while the other two belong to the Santa Iría formation. Polished thin-sections cut perpendicularly to the foliation were analyzed at the Institut de Minéralogie, de Physique des Matériaux et de Cosmochimie at the Sorbonne University of Paris (France). We followed closely the analytical procedure described by Beyssac et al. (2002a, b; 2003; see supplementary information). More than 15 Raman spectra (Fig. 3) were obtained for each sample using a Renishaw InVIA Reflex microspectrometer equipped with a 514.5 nm Modulaser argon laser under circular polarization. The laser was focused by a DMLM Leica microscope, and laser power was set below 1 mW at the sample surface. The Rayleigh diffusion was eliminated by edge filters and the signal was dispersed using a 1800 g/mm grating and finally analyzed by a Peltier cooled RENCAM CCD detector. The recorded spectral window was large to correctly set the background correction, from 700 to 2000 $cm^{-1}$ in case of low-temperature samples. Before each session, the spectrometer was calibrated with a silicon standard. CM was systematically analyzed behind a transparent adjacent mineral, generally quartz or white mica grains oriented along $S_1$. For a full description of the temperature calculations see the supplementary information.

## 4. Results

According to the petrographic study, all the samples correspond to slates or phyllites with phyllosilicates smaller than 500 μm, composed of variable quartz + K-white mica ± chlorite ± feldspar ± ore and accessory minerals (Fig. 2d-f). Samples from the Santa Iría formation have much smaller grain-size and apparently lower "crystallinity" (Fig. 2f). The first foliation $S_1$ is defined by the largest micas and chlorites (Fig. 2d-e), being folded by microscopic- to centimetric-scale tight folds of the second deformation phase (Fig. 2a-b, d-e). The second foliation $S_2$ is the main foliation at outcrop (Fig. 2a-c), but the development of phyllosilicates (mostly white mica) is lesser than $S_2$. The third foliation $S_3$ is much less penetrative (Fig. 2a-c) and does not develop phyllosilicates.

### 4.1. X-Ray diffraction

The mineralogy and crystal parameters of K-white mica obtained from the 18 samples of the Pulo do Lobo domain are summarized in Table 1. The results of KI values, b-cell parameter and $d_{001}$ analyzed in K-white mica, obtained from whole-rock and <2 μm fractions are very similar, which suggests that detrital micas re-equilibrated during metamorphism.

The mineralogy of the samples is relatively simple: Qz + Ms + Fsp+ Chl ± Pg ± C/S. The slates of the Santa Iría formation have quartz, muscovite and chlorite, with chlorite/smectite interlayers (C/S) in some samples. In the lower formations, besides quartz and muscovite, chlorite is present in almost all of the samples, paragonite appears in most of them, and chlorite/smectite interlayers are occasional.

KI values measured in the 10 Å peak of white mica from the <2 μm fraction are shown in Table 1 and Fig. 1c with a relative colour bar from orange (lower values) to green (higher values). Values of the Santa Iría samples (n=5) range from 0.20 to 0.26 $\Delta°2\theta$, the mean value being 0.23 (standard deviation 0.02). As for the lower formations (n=12), KI values range from 0.17 to 0.22, the mean value being 0.19 (standard deviation 0.02). KI values measured in the 5 Å peak (not shown) are very similar to those of the 10 Å peak.

The measured *b*-cell parameter of white mica varies in a close range around 9 Å (8.991-9.002). Mean value is 8.995 Å (standard deviation 0.003) for the Santa Iría formation samples, and 8.997 Å (standard deviation 0.003) for the samples of the lower formations. $d_{001}$ values average 9.992 Å (standard deviation 0.004) and differ slightly between upper and lower formations, being higher in the upper formation.

The results obtained through X-Ray diffraction denote low-grade metamorphic conditions due to the KI values between 0.17-0.26 $\Delta°2\theta$. In addition, *b*-cell parameters are lower than 9.000 Å which show a low-pressure metamorphic gradient (low pressure/temperature metamorphic facies conditions; Guidotti and Sassi, 1986).

### 4.2. Compositional maps and chlorite thermometry

X-Ray maps show the distribution of major elements and allow identifying white mica, chlorite, and some albite porphyroblasts, with ilmenite and rutile as accessory minerals (Fig. 4a-b). Although quartz is abundant in all of the samples, the zoomed selected areas for X-ray mapping (composed mostly by phyllosilicates) do not contain quartz (Fig. 4a-b). White mica is abundant along both $S_1$ and $S_2$ foliations (Fig. 2d-e and 4b). Chlorite is found mostly along $S_1$, being very scarce and small-sized along $S_2$ (Fig. 2e and 4b), with the exception of sample PLB-93 where chlorite is similar in amount in both foliation domains (Fig. 4b).

Mapped compositions of end-members of white mica and chlorite have been plotted in the ternary diagrams of Figure 5. The composition of white mica is similar in the three maps. It is close to muscovite, with 25% of pyrophyllite and very scarce celadonite content (0-10%; Fig. 5a). The high content of pyrophyllite (high amount of interlayer vacancies) is typical of low-pressure illitic-mica compositions. Figure 6 shows white mica compositional ratios, which can be related to P/T conditions: they present low degree of Na substitution and low phengitic component, thus being close to the muscovite end-member. These results point to low-pressure conditions and agree well with XRD results: low *b*-cell parameter (< 9.000 Å) and high $d_{001}$ (> 9.985 Å; Table 1).

Chlorite compositions are variable, though all of them have in common ≈50% clinochlore + daphnite and ≈50% amesite + sudoite (Fig. 5b). Chlorites in sample PLB-88 are poor in amesite with a large variation of clinochlore + daphnite and sudoite. In sample PLB-84 chlorites, variable compositions between amesite and sudoite indicate a variation of $Al^{IV}$, which implies an increase of temperature from rims to cores as shown in the chemical maps of Fig. 4c. Finally, PLB-93 chlorites are poor in sudoite and higher in $Al^{IV}$ content, thus suggesting higher average temperatures (Vidal et al., 2006). Altogether, chlorite compositional data suggest the presence of two end-members: sudoite-rich low-temperature (PLB-88), and amesite-rich high-temperature (PLB-93).

Maps of $Al^{IV}$ in chlorites have been represented in Fig. 4c. Sample PLB-88 shows lower $Al^{IV}$ content (≈1.1-1.3 apfu) than sample PLB-93 (≈1.3-1.5 apfu). In sample PLB-84, some large chlorite grains oriented along $S_1$ are zoned, with higher $Al^{IV}$ content in the cores (≈1.4 apfu) than in the rims (≈1.0 apfu; see white square in Fig. 4c). According to the empirical calibration of Cathelineau (1988), $Al^{IV}$ in chlorites increases with temperature. Thus, the $Al^{IV}$ content in chlorites manifests different temperatures in different samples, and also from core to rim in singular grains.

Temperature maps have been obtained with the semi-empirical thermometer of Lanari et al. (2014b), assuming that $Fe^{2+}$ is the Fe total (Fig. 4d). Temperatures range between 100-200 °C in sample PLB-88, 150-350 °C in sample PLB-84, and 200-450 °C in sample PLB-93. Tiny chlorites developed along $S_2$ show lower temperatures than larger and more abundant chlorites along $S_1$, with the exception of sample PLB-93. Furthermore, some large chlorites oriented along $S_1$ are zoned, showing high-temperature relic cores (350-450 °C; see white insets in Fig. 4c-d) surrounded by low-temperature rims (150-250 °C).

To test Vidal et al. (2005, 2006) and Bourdelle et al. (2013) approaches, an area of representative chlorites in an $S_1$ microlithon was selected from each map (see red insets in Fig. 4d). Corresponding chlorite compositions were extracted and introduced in the chlorite-quartz-water equilibria (Fig. 7a, Vidal et al., 2005, 2006; Fig. 7b, Bourdelle et al., 2013). The

448 temperature estimates (Fig. 7) are fairly similar with both methods, averaging 120-230 °C in
449 sample PLB-88 and 150-380 °C in sample PLB-84. This is also in agreement with the
450 temperature maps calculated with the Lanari et al. (2014a) model. Only the sample PLB-93
451 shows a divergence on temperature averages: mostly 150-250 °C with the thermometer of
452 Bourdelle et al. (2013), and 250-350 °C with the one of Vidal et al. (2005, 2006). In both
453 cases (Bourdelle et al. (2013) and Vidal et al. (2005, 2006) approaches), the higher
454 temperature analyses are obtained from crystal cores and belong mostly to the sample PLB-
455 93.

456

457 **4.3. RSCM thermometry**

458 The ratio parameters and corresponding maximum temperatures obtained from all the
459 spectra analyzed are shown in the supplementary information. The Raman spectra were
460 decomposed into bands following the appropriate fitting procedure described in Beyssac et
461 al. (2002a) for the lower formations (high-temperature Raman spectra; ratio parameter R2)
462 and Lahfid et al. (2010) for the Santa Iría formation (low-temperature Raman spectra; ratio
463 parameters RA1 and RA2; Fig. 3). The average temperatures are shown in Table 1 and Fig.
464 1c with a relative colour bar from red (higher temperature) to blue (lower temperature). The
465 average temperatures for the lower formations range from 420 to 530 °C, with a mean value
466 of 468 °C (standard deviation of 35). The highest temperatures are found in samples PLB-
467 82 (530 °C) and PLB-93 (495 °C), while the remaining ones do not exceed 480 °C. As for
468 the Santa Iría formation, temperatures are lower (315-330 °C; Table 1) than in the underlying
469 formations.

470

471 **5. Interpretation and discussion**

472 **5.1. Deformation/metamorphism relationships**

473 The obtained analytical results must be interpreted in the context of the Variscan evolution
474 of the Pulo do Lobo domain. As described above, two regional deformational events $D_1$ and
475 $D_2$ gave way to the development of foliations (Devonian $S_1$ and Carboniferous $S_2$)
476 accompanied by metamorphic phyllosilicate growth ($M_1$ and $M_2$). In the cross-sections of
477 Fig. 1c, KI values derived from XRD and average temperature from RSCM suggest that the
478 lowest metamorphic grade (green and blue colours) corresponds to the Santa Iría formation.

479 The textural observations evidence that in most samples of the lower formations $M_1$ was the
480 main crystallization event, developing abundant and large-sized white mica and chlorite in $S_1$
481 microlithons, while $M_2$ gave way to small-sized white mica (e.g., Fig. 2e and map 1 in Fig. 4).
482 On the other hand, polydeformed rocks commonly show previously grown minerals rotated
483 towards a new foliation developed at lower-grade conditions, without new crystallization.
484 This can be the case of the white micas that define $S_2$ in some samples (illustrated in Fig. 2d),
485 which, in turn, is not contradictory with the similar chemical composition of $S_1$ and $S_2$ micas
486 (Fig. 5a). As shown in these samples, $S_1$ is variably crenulated by $D_2$, so that $M_1$ minerals are
487 variably rotated towards $S_2$. Consequently, the metamorphic data obtained from the samples
488 of the lower formations will be ascribed to $D_1$-$M_1$. Sample PLB-93 might represent an
489 exception, since its slightly higher RSCM and chlorite-derived temperatures might be due to

nearby intrusions (Fig. 1b and 1c.1). At this respect, it is important to note the Mississippian transtensional event (basins development and abundant mafic magmatism) that took place between $D_1$ and $D_2$ (Pérez-Cáceres et al., 2015). The characterization of $M_2$ can be done by studying the samples from the Santa Iría formation, which are only affected by $S_2$ accompanied by small-sized phyllosilicate growth (Fig. 2f). No crystallization has been observed related to the S3 disjunctive crenulation cleavage.

### 5.2. First tectonothermal event (Devonian $M_1$)

The observed mineral association (Qz + Ab + Ms + Chl ± Pg), together with the presence of C/S is compatible with low-grade metamorphic conditions (Table 1). White mica "crystallinity" values (0.17-0.22 Δ°2θ; average 0.19) are always in the range of the epizone (low-grade or greenschists facies; >300 °C; Frey, 1987; Kisch, 1987, Warr and Ferreiro Mählnlmann, 2015), in accordance with the values reported by Abad et al. (2001) in a more general study of the diagenetic-metamorphic evolution of the South Portuguese Zone metapelites. Nevertheless, both the values of KI, still far from 0.14 Δ°2θ (high epizone conditions according to Abad et al., 2006), and their variability, suggest that temperature was not high enough as to stabilize a highly crystalline white mica. This is in agreement with the low Na content of K-micas coexisting with paragonite (Fig. 6), meaning a very-low temperature position in the muscovite-paragonite solvus for natural quasi-binary Pg-Ms pairs (Guidotti et al., 1994). By contrast, the maximum temperatures obtained with RSCM geothermometry are surprisingly high (420-530 °C; average 470 °C; corresponding to very high epizone or even medium-grade conditions; Table 1).

The composition of paired chlorite and white mica is normally used to calculate pressure and temperature (e.g., Vidal et al., 2006), but multi-equilibrium approach was not successful because the P-T equilibrium conditions did not converge. This result is indicative of chemical disequilibrium, precluding their use as a reliable geothermobarometer in this case. The temperatures calculated from chlorite compositions following various approaches (Vidal et al., 2006, Fig. 7a; Bourdelle et al., 2013, Fig. 7b; Lanari et al., 2014a, Fig. 4d) are as follow: 100-230 °C for sample PLB-88, 150-375 °C for sample PLB-84, and 150-450 °C for sample PLB-93 (Figs. d and 7, and Table 1). The slightly higher temperature of sample PLB-93 is inferred from its highest white mica "crystallinity" (0.17 Δ°2θ), high RSCM temperature (495 °C), high-temperature (amesite-rich) chlorite and higher chlorite thermometry (Table 1), and can be explained by its nearness to metric-scale mafic igneous bodies of the Peramora Mélange (located at ≈200 m to the south; Pérez-Cáceres et al., 2015) and/or to a granite stock (located at ≈5 km to the west) (Fig. 1b).

In our samples there is some evidence of chlorite retrogression: (i) the chemical disequilibrium showed by the white mica/chlorite geothermobarometer, (ii) the presence of C/S mixed layers not stable in the epizone (e.g. Potel et al., 2006), (iii) the difference between temperature estimates from crystal rims to cores, and the higher temperature relic cores preserved in large chlorites defining $S_1$ (Fig. 4c-d), and (iv) the previously reported XRD and TEM data of chlorite retrograded to smectite and corrensite in the Pulo do Lobo domain (see fig. 1 in Nieto et al., 2005). The existence of chlorites with different compositions crystallized at different temperatures is the usual scenario (e.g., Vidal et al., 2006, 2016; Lanari

et al., 2012; 2014a and b; Grosch et al., 2012; 2014; Cantarero et al., 2014). In such situation, the definition of a single temperature and pressure attributable to peak conditions is really difficult. The maximum temperature showed by chlorite relic cores is 350-450 °C (Fig. 4d), which is more in accordance with the conditions estimated for $M_1$ by means of RSCM data.

An issue that deserves some discussion is the difference in temperature estimates between RSCM and other techniques. RSCM thermometry records the peak temperature and is not sensitive to the retrograde path. Alternatively, other methods based on phyllosilicate compositions are prone to record reequilibration during the retrograde path; thus, they rarely record the peak conditions, except perhaps in the core of certain large crystals. Therefore, RSCM and phyllosilicate-based methods do not record the same information on temperature, being in fact complementary. The analyzed CM grains were carefully checked by microtextural observation and spectral geometry to make sure that these grains are actually derived from in situ organic matter graphitized during metamorphism.

In our case study, at the high peak temperature given by the RSCM thermometry, minerals such as biotite or garnet are expected to crystallize in metasediments, though they have not been observed in our samples. Biotite has been said to exist in a few previous works (Apalategui et al., 1983; Braid et al., 2010; Rubio Pascual et al., 2013). However, in a few of our samples, biotite-looking crystals have resulted to be oxichlorites under SEM analyses. The absence or exceptional presence of biotite can be due to whole-rock composition, and explained by growth inhibition related to Na-excess, as evidenced by the presence of albite and paragonite in our samples. Another possible explanation could be the higher sensitivity of CM graphitization to fast reequilibration during a short-time thermal event. Thus, the Mississippian intrusions subsequent to $M_1$ in the Pulo do Lobo formation (see description in section 2) could have exerted a fast and locally intense thermal imprint that influenced CM but not the crystal chemistry of silicates. Moreover, recrystallization processes are not only function of temperature, but also promoted by deformation/stress, time, fluid/rock ratio (Merriman and Frey, 1999). Observations of this kind (differing reaction kinetics between organic and inorganic material (e.g. illite) in a contact metamorphic setting can be found in Olsson (1999) and Abad et al. (2014). Regarding the time of geological processes, Mori et al. (2017) investigated the importance of heating duration for RSCM thermometry by studying graphitization around dykes. They showed that small-scale intrusions generating short thermal events modify the structure of CM in the surrounding rocks, to conclude that CM crystallinity is clearly related to contact metamorphism. The influence of low-pressure contact aureoles on RSCM temperature patterns is further supported by the results obtained by Hilchie and Jamieson (2014), who concluded that the variation of RSCM temperatures can be controlled by the subsurface geometry of a pluton. Finally, the long-distance thermal influence of plutonic intrusions on low-grade rocks located as far as 10 km has already been evidenced (e.g., Merriman and Frey, 1999; Martínez Poyatos et al., 2001) and could also be recorded by RSCM thermometry in our samples.

### 5.3. Second tectonothermal event (middle/upper Carboniferous $M_2$)

The mineralogy of the Santa Iría samples (Qz + Fsp + Ms + Chl ± C/S) is compatible with very low- to low-grade conditions. The K-white mica "crystallinity" values (0.20-0.26 Δ°2θ;

576 average 0.23) point to lower epizone conditions, very close to the boundary with the
577 anchizone (≈300 °C; Frey, 1987; Kisch, 1987). The temperatures calculated by RSCM in two
578 samples (315 and 330 °C) are compatible with the KI data of XRD analysis.

579 Our metamorphic data corroborate the existence of an unconformity between the lower and
580 upper formations of the Pulo do Lobo domain (Pérez-Cáceres et al., 2015). Table 2
581 summarizes the relationship between deformation and metamorphism of the Pulo do Lobo
582 domain in the context of the Variscan tectonic evolution of SW Iberia (Pérez-Cáceres et al.,
583 2015). The lower formations record a Devonian tectonothermal event that reached epizone
584 or lower greenschist facies conditions ($M_1$ with generalized phyllosilicate growth at
585 temperatures as high as 450 °C), while the overlying upper formation records a middle/upper
586 Carboniferous tectonothermal event close to the anchizone/epizone boundary ($M_2$ with
587 small-sized phyllosilicate growth at temperatures ≈300-330 °C; Table 1). Obviously, $M_2$ also
588 affected somehow the lower formations, being, at least in part, the responsible for the
589 observed retrogression of $M_1$ chlorite and/or crystallization of new chlorites at lower
590 temperature.

591

592 **5.4. Pressure conditions**

593 The measured *b*-cell parameters of K-white mica (in a short range between 8.991-9.002 Å;
594 average 8.996; standard deviation 0.003) are very similar in the lower and upper formations
595 of the Pulo do Lobo domain. Thus, the *b* parameter is consistently homogeneous and reflects
596 very low phengite substitution in mica, as expected at low-pressure settings (Potel et al., 2006,
597 2016), near the intermediate pressure gradient boundary (Guidotti and Sassi, 1986).

598 In agreement with the low *b*-cell parameters, the composition of K-white mica is close to
599 muscovite with very low celadonite and higher pyrophyllite content (Fig. 5a), as expected for
600 illite-rich mica formed at low-pressure gradients. In the case of high- or medium-pressure
601 conditions, a continuous trend in mica compositions would be found reflecting the
602 decompression path after the peak pressure, while the *b*-cell parameter would represent an
603 average value of the range of mica compositions found in the sample (Abad et al., 2003b).
604 On the contrary, at low-pressure settings, the overall range of recorded pressure is very short
605 and micas present similar compositions and *b*-cell parameters among the various samples, as
606 in the case of the Pulo do Lobo samples (Figs. 5a and 6, and Table 1).

607 The Pulo do Lobo domain has been classically interpreted as a pre-collisional subduction-
608 related accretionary prism, based on the MORB geochemistry of their mafic rocks (see
609 section 2.1). According to this classical interpretation, features typical of modern subduction
610 systems should be expected, such as high-pressure metamorphic gradient remnants of partial
611 subduction/exhumation in an accretionary wedge (e.g., Platt, 1986; Ernst, 2005), or slices of
612 oceanic slab-derived lithologies (varied mid-ocean ridge metaigneous lithologies and also
613 deep ocean bottom metasediments). Thus, recent works on the Makran accretionary prism
614 (Omrani et al., 2017) and the subduction system of Japan (Endo and Wallis, 2017) describe
615 an accretionary mélange complex composed of pelagic sedimentary rocks, ophiolites,
616 greenschists, amphibolites, and blueschists with high-pressure minerals such as lawsonite and
617 glaucophane. On the contrary, most of the geological data concerning the Pulo do Lobo

618 domain do not back up such interpretation (see section 2.1), and our new results about
619 pressure conditions are also in disagreement. The only suspect of high-pressure gradient in
620 the Pulo do Lobo domain is the interpretation of some rhomboidal aggregates of epidote
621 porfiroblasts as the remnants of supposed lawsonite grown previously to $S_2$ in some samples
622 of Pulo do Lobo mafic schists (Rubio Pascual et al., 2013). However, no analytical data have
623 been presented to support the lawsonite pseudomorphs.

624

625 **6. Conclusions**

626 Eighteen samples of metapelites from the Pulo do Lobo domain have been studied to
627 characterize their Variscan low-grade metamorphism. The microstructural analysis of the
628 samples of the lower formations (Devonian Pulo do Lobo and Ribeira de Limas) shows the
629 existence of two superposed low-grade tectonothermal events with associated foliation and
630 phyllosilicate growth ($S_1$-$M_1$ and $S_2$-$M_2$; Table 2). $M_2$ was less intense, being the only event
631 that affected the overlying Carboniferous Santa Iría formation. The regional geology also
632 shows that a Mississippian thermal (magmatic-derived) event occurred in-between $M_1$ and
633 $M_2$.

634 $M_1$ and $M_2$ correspond to the chlorite zone, but $M_1$ entered the epizone (greenschists facies
635 with temperatures up to ≈450 °C), while $M_2$ did not exceed the anchizone-epizone boundary
636 (≈300 °C).

637 The temperatures obtained from RSCM are higher compared to the ones derived from
638 chlorite geothermometry and white mica data. The discrepancy can be explained by the fact
639 that RSCM records the true maximum temperature, being not affected by retrogression as
640 other methods do. In addition, this difference can be the consequence of the high sensitivity
641 of CM to quickly equilibrate at maximum temperatures during short thermal events due to
642 magmatic intrusions emplaced during the Mississippian thermal event.

643 Thermodynamic disequilibrium between white mica and chlorite has precluded their use for
644 geothermobarometry, and a variety of data (including the existence of relic high-temperature
645 chlorite cores, the presence of chlorite/smectite mixed layers, or the very-low temperatures
646 calculated with chlorite geothermometers) indicate chlorite retrogression after $M_1$
647 metamorphic climax and crystallization of new chlorite grains at lower temperature.

648 The low-pressure conditions derived from white mica indicators (very low celadonite content
649 and *b*-cell values) are incompatible with the high-pressure metamorphic gradient expected in
650 a subduction-related accretionary wedge, which has been the classical interpretation of the
651 Pulo do Lobo domain.

652

653

654 **Acknowledgements**

655 This work was supported by the projects CGL2011-24101 (Spanish Ministry of Science and
656 Innovation), CGL2015-71692-P and CGL2016-75679-P (Spanish Ministry of Economy and
657 Competitiveness), RNM-148 and RNM-179 (Andalusian Government) and BES-2012-

055754 (Doctoral scholarship to I. Pérez-Cáceres from the Spanish Ministry of Science and Innovation). The Raman facility in Paris has been funded by the City of Paris (Emergence program). We thank Valérie Magnin for her assistance with the microprobe analysis in Grenoble and Pierre Lanari for his support with thermodynamic software. Detailed revisions by C. Quesada and an anonymous reviewer contributed to improve this paper.

## Figure captions

**Figure 1**. a) Location of the studied area in the SW of the Iberian Massif (in grey). CIZ: Central Iberian Zone, OMZ: Ossa-Morena Zone, SPZ: South Portuguese Zone. b) Geological map of the Pulo do Lobo domain and other units related to the OMZ/SPZ boundary with indications of the two cross-sections studied and collected samples. c.1-2) Geological cross-sections of the Pulo do Lobo domain (see b for location) (modified from Martínez Poza et al., 2012 and Pérez-Cáceres et al., 2015). Numbered red circles in b-c locate the samples studied. Big circles show the KI values for 10 Å reflection peaks of K-white mica and the average RSCM temperatures, with the relative colour bar according to the results shown in Table 1. BAA: Beja-Acebuches Amphibolites, M: metabasalts, PL: Pulo do Lobo formation, RL: Ribeira de Limas formation, SI: Santa Iría formation.

**Figure 2**. Pictures of the Pulo do Lobo rocks illustrating deformation at outcrop scale: a) Pulo do Lobo formation, b) Ribeira de Limas formation, c) Santa Iría formation. Microphotographs from thin-sections: d) Cross-polarized light image of sample PLB-84 (Pulo do Lobo formation), e) SEM-BSE image of sample PLB-88 (Ribeira de Limas formation), f) Cross-polarized light images of sample PLB-71 (Santa Iría formation).

**Figure 3**. Representative Raman spectra of CM across the Pulo do Lobo domain from low temperature (bottom; Santa Iría formation) to high temperature (top; lower formations) including the average maximum temperatures (ºC) for each sample. Vertical scale for spectrum intensity is arbitrary. See Fig. 1 for sample location and Table 1 and supplementary information for RSCM data.

**Figure 4**. X-Ray maps of the three selected samples analyzed by EPMA and processed with XMapTools. The samples belong to the lower formations of the Pulo do Lobo domain (sample PLB-88: Ribeira de Limas formation; samples PLB-84 and PLB-93: Pulo do Lobo formation; the latter (PLB-93) is close to Early Carboniferous igneous intrusions). a) EPMA BSE photographs. b) Mineral maps. c) $Al^{IV}$ content map in chlorites, which increases with temperature. The white square highlights the zonation of a chlorite grain from core to rim. d) Temperature maps of chlorite using the Lanari et al. (2014a) geothermometer assuming all iron as ferrous. White squares show selected areas illustrating higher-temperature chlorite cores. Red squares show the selected areas (representative of $S_1$ foliation) used for chlorite-quartz-water geothermometric calculations shown in Fig. 7.

**Figure 5**. Ternary plots of all the analyzed white micas (a) (Cel: celadonite, Mus: muscovite, Prl: pyrophyllite) and chlorite (b) (Cli+Daph: clinochlore + daphnite, Am: amesite, Sud: sudoite) plotted with the XmapTools TriPlot3D module. Colour bars refer to the number of mica/chlorite pixels analyzed.

**Figure 6**. Compositional diagram of white micas showing Na/Na+K vs Si/Al (atomic ratios) for 31 EPMA point analyses from seven samples of the lower formations of the Pulo do Lobo domain (different symbology, for each sample). Point analyses were obtained on the microprobe at the University of Huelva (Spain). Qualitative information about temperature and pressure conditions are respectively according to Guidotti et al. (1994), Coggon and Holland (2002), Parra et al. (2002), Massonne and Schereyer (1987) and Massonne and Szpurka (1997).

**Figure 7**. Histograms of temperatures obtained using the chlorite-quartz-water geothermometer of Vidal et al. (2006) (a) and Bourdelle et al. (2013) (b) on selected representative $S_1$ chlorites (see red squares in Fig. 4d for location). *n* represents the number of chlorites that could be used for each calibration. The number of analyses is lower in those with Vidal et al. (2006) approach because the assumption that the Si content of chlorite is lower than 3 apfu.

## Table captions

**Table 1**. Samples and results obtained by XRD (<2 μm fraction), white mica and chlorite compositions, temperature ranges from chlorite thermometry, and average RSCM thermometry. Basel KI values and average RSCM temperatures show a relative colour-bar scale. Mineral abbreviations according to Whitney & Evans (2010). Qz: Quartz, Ms: Muscovite, Fsp: Feldspar, Chl: Chlorite, Pg: paragonite, C/S: chlorite-smectite mixed layers, Cel: celadonite, Prl: pyrophyllite, Cli+Daph: clinochlore + daphnite, Am: amesite, Sud: sudoite, Std Dv: standard deviation.

**Table 2.** Summary of the tectonometamorphic Variscan evolution of the Pulo do Lobo domain.

## References


Abad, I., Mata, M.P., Nieto, F., and Velilla, N: The phyllosilicates in diagenetic-metamorphic rocks of the South Portuguese Zone, southwestern Portugal, The Canadian Mineralogist, 39(6), 1571-1589, 2001.

Abad, I., Nieto, F., and Velilla, N.: Chemical and textural characterisation of diagenetic to low-grade metamorphic phyllosilicates in turbidite sandstones of the South Portuguese Zone: A comparison between metapelites and sandstones, Schweizerische Mineralogische und Petrographische Mitteilungen, 82(2), 303-324. 2002.

Abad, I., Nieto, F., and Gutiérrez-Alonso, G.: Textural and chemical changes in slate-forming phyllosilicates across the external-internal zones transition in the low-grade metamorphic belt of the NW Iberian Variscan Chain, Swiss Bulletin of Mineralogy and Petrology, 83(1), 63-80, 2003a.

Abad, I., Gutierrez-Alonso, G., Nieto, F., Gertner, I., Becker, A., and Cabero, A.: The structure and the phyllosilicates (chemistry, crystallinity and texture) of Talas Ala-Tau (Tien Shan, Kyrgyz Republic); comparison with more recent subduction complexes, Tectonophysics, 365(1-4), 103-127, 2003b.

Abad, I., Nieto, F., Gutiérrez-Alonso, G., Campo, M. D., López-Munguira, A., and Velilla, N.: Illitic substitution in micas of very low-grade metamorphic clastic rocks. European Journal of Mineralogy, 18(1), 59-69, 2006.

Abad, I., Nieto, F., Velilla, N., and Suárez-Ruiz, I.: Metamorphic evidences from the Monchique pluton (South Portugal): Contact metamorphism vs regional metamorphism under very low-grade conditions, Revista de la Sociedad Geológica de España, 27(1): 337-350, 2014.

Abalos, B., Gil Ibarguchi, J.I., and Eguiluz, L.: Cadomian subduction/collision and Variscan transpression in the Badajoz-Córdoba shear belt, southwest Spain, Tectonophysics, 199, 51-72, 1991.

743 Airaghi, L., Lanari, P., de Sigoyer, J., and Guillot, S.: Microstructural vs compositional preservation
744 and pseudomorphic replacement of muscovite in deformed metapelites from the Longmen
745 Shan (Sichuan, China), Lithos, 282, 262-280, 2017.

746 Ali, A.: The tectono-metamorphic evolution of the Balcooma Metamorphic Group, north-eastern
747 Australia: a multidisciplinary approach, Journal of Metamorphic Geology, 28(4), 397-422,
748 2010.

749 Apalategui, O., Barranco, E., Contreras, F., Delgado, M., and Roldán, F. J.: Hoja 916, Aroche, Mapa
750 Geológico de España a escala 1:50000, Inst. Geológico y Minero de España, Madrid, 1983.

751 Araújo, A., Fonseca, P., Munhá, J., Moita, P., Pedro, J., and Ribeiro, A.: The Moura Phyllonitic
752 Complex: an accretionary complex related with obduction in the southern Iberia Variscan
753 suture, Geodinamica Acta, 18, 375-388, 2005.

754 Arenas, R., Abati, J., Martínez Catalán, J.R., García, F. D., and Pascual, F.R.: PT evolution of eclogites
755 from the Agualada Unit (Ordenes Complex, northwest Iberian Massif, Spain): Implications
756 for crustal subduction, Lithos, 40(2), 221-242, 1997.

757 Azor, A., González Lodeiro, F., and Simancas, J.F.: Tectonic evolution of the boundary between the
758 Central Iberian and Ossa-Morena zones (Variscan Belt, southwest Spain), Tectonics, 13, 45-
759 61, 1994.

760 Azor, A., Rubatto, D., Simancas, J.F., González Lodeiro, F., Martínez Poyatos, D., Martín Parra L.M.,
761 and Matas, J.: Rheic Ocean ophiolitic remnants in Southern Iberia questioned by SHRIMP
762 U-Pb zircon ages on the Beja-Acebuches amphibolites, Tectonics, 27(5), 2008.

763 Azor, A., Simancas, J.F., Martínez Poyatos, D., Pérez-Cáceres, I., González Lodeiro, F., and Expósito,
764 I.: Chapter 10.3: Deformation and Structure, Southwestern Iberia, in: The Geology of Iberia:
765 A Geodynamic Approach, Volume 2: The Variscan Cycle, edited by: Quesada, C., and
766 Oliveira, J.T., Springer, 316-335, 2019.

767 Barbero, L.: Granulite-facies metamorphism in the Anatectic Complex of Toledo, Spain: late
768 Hercynian tectonic evolution by crustal extension, Journal of the Geological Society, 152(2),
769 365-382, 1995.

770 Bard, J.P. : Signification tectonique des métatholeites d'anité abyssale de la ceinture de base pression
771 d'Aracena (Huelva, Espagne), Bulletin de la Société Géologique de France, 19, 385-393,
772 1977.

773 Bastida, F., Martínez-Catalán, J.R., and Pulgar, J.A.: Structural, metamorphic and magmatic history
774 of the Mondoñedo nappe (Hercynian belt, NW Spain). Journal of Structural Geology, 8(3-
775 4), 415-430, 1986.

776 Bastida, F., Brime, C., García-López, S. Aller, J., Valin, M.L., and Sanz-López, J.: Tectono-thermal
777 evolution of the Cantabrian Zone (NW Spain), in: Palaeozoic conodonts from northern
778 Spain, edited by: García López, S., and Bastida, F., Instituto Geológico y Minero de España,
779 Cuadernos del Museo Geominero, 1, 105-123, Madrid, ISBN: 84-7840-446-5, 2002.

780 Battaglia, S., Leoni, L., and Sartori, F.: The Kübler index in late diagenetic to low-grade metamorphic
781 pelites: a critical comparison of data from 10 Å and 5 Å peaks, Clays and Clay Minerals,
782 52(1), 85-105, 2004.

783 Beyssac, O., Goffé, B., Chopin, C., and Rouzaud, J.N.: Raman spectra of carbonaceous material in
784 metasediments: a new geothermometer, Journal of Metamorphic Geology, 20, 859-871,
785 2002a.

786 Beyssac, O., Rouzaud, J.-N., Goffé, B., Brunet, F., and Chopin, C.: Graphitization in a high-pressure,
787 low temperature metamorphic gradient: a Raman microspectroscopy and HRTEM study.
788 Contrib. Mineral. Petrol., 143, 19-31, 2002b.

789 Beyssac, O., Goffé, B., Petitet, J.P., Froigneux, E., and Rouzaud, J.N.: On the characterization of
790 disordered and heterogeneous carbonaceous materials using Raman spectroscopy,
791 Spectrochim. Acta A Mol. Biomol. Spectrosc., 59, 2267-2276, 2003.

792 Beyssac, O., Bollinger, L., Avouac, J.P., and Goffé, B.: Thermal metamorphism in the lesser Himalaya
793 of Nepal determined from Raman spectroscopy of carbonaceous material, Earth and
794 Planetary Science Letters, 225, 233-241, 2004.

795 Booth-Rea, G., Simancas, J.F., Azor, A., Azañón, J.M., Gonzalez Lodeiro, F., and Fonseca, P.: HP-
796 LT Variscan metamorphism in the Cubito-Moura schists (Ossa-Morena Zone, southern
797 Iberia), Comptes Rendus Geoscience, 338(16), 1260-1267, 2006.

798 Bourdelle, F., Parra, T., Chopin, C., and Beyssac, O.: A new chlorite geothermometer for diagenetic
799 to low-grade metamorphic conditions, Contributions to Mineralogy and Petrology, 165(4),
800 723-735, 2013.

801 Bousquet, R., Oberha, R., Goffé, B., Wiederkehr, M., Koller, F., Schmid, S.M., Schuster, R., Engi,
802 M., Berger, A., and Martinotti, G.: Metamorphism of metasediments at the scale of an
803 orogen: a key to the tertiary geodynamic evolution of the Alps, Geological Society, London,
804 Special Publications, 298, 393-411, 2008.

805 Braid, J.A., Murphy, J.B., and Quesada, C.: Structural analysis of an accretionary prism in a continental
806 collisional setting, the Late Paleozoic Pulo do Lobo Zone, Southern Iberia, Gondwana
807 Research, 17(2-3), 422-439, 2010.

808 Braid, J. A., Murphy, J. B., Quesada, C., and Mortensen, J.: Tectonic escape of a crustal fragment
809 during the closure of the Rheic Ocean: U–Pb detrital zircon data from the Late Palaeozoic
810 Pulo do Lobo and South Portuguese zones, southern Iberia, Journal of the Geological
811 Society, 168(2), 383-392, 2011.

812 Braid, J. A., Murphy, J. B., Quesada, C., Gladney, E. R. and Dupuis, N.: Progressive magmatism and
813 evolution of the Variscan suture in southern Iberia. International Journal of Earth Sciences,
814 107(3), 971-983, 2018.

815 Brown, M.: P–T–t evolution of orogenic belts and the causes of regional metamorphism, Journal of
816 the Geological Society, 150(2), 227-241, 1993.

817 Burg, J.P., Iglesias, M., Laurent, P., Matte, P., and Ribeiro, A.: Variscan intracontinental deformation:
818 the Coimbra-Córdoba Shear zone (SW Iberian Peninsula), Tectonophysics, 78, 161-177,
819 1981.

820 Cantarero, I., Lanari, P., Vidal, O., Alías, G., Travé, A., and Baqués, V.: Long-term fluid circulation
821 in extensional faults in the central Catalan Coastal Ranges: P–T constraints from neoformed
822 chlorite and K-white mica, International Journal of Earth Sciences, 103(1), 165-188, 2014.

823 Castro, A., Fernández, C., De la Rosa, J.D., Moreno Ventas, I., and Rogers, G.: Significance of
824 MORB-derived amphibolites from the Aracena metamorphic belt, southwest Spain, Journal
825 of Petrology, 37(2), 235-260, 1996.

826 Castro, A., Fernández, C., El-Hmidi, H., El-Biad, M., Díaz, M., De la Rosa, J., and Stuart, F.: Age
827 constraints to the relationships between magmatism, metamorphism and tectonism in the
828 Aracena metamorphic belt, southern Spain, International Journal of Earth Sciences, 88(1),
829 26-37, 1999.

Cathelineau, M.: Cation site occupancy in chlorites and illites as a function of temperature, Clay Minerals 23, 471-485, 1988.

Cathelineau, M., and Nieva, D.: A chlorite solid solution geothermometer the Los Azufres (Mexico) geothermal system, Contrib. Mineral Petrol., 91(3), 235-244, 1985.

Coggon, R., and Holland, T.J.B.: Mixing properties of phengitic micas and revised garnet-phengite thermobarometers, Journal of Metamorphic Geology, 20(7), 683-696, 2002.

Crespo-Blanc, A. and Orozco, M.: The Southern Iberian Shear Zone: a major boundary in the Hercynian folded belt. Tectonophysics, 148(3-4), 221-227, 1988.

Crespo-Blanc, A.: Evolución geotectónica del contacto entre la zona de Ossa-Morena y la zona Surportuguesa en las sierras de Aracena y Aroche (Macizo Ibérico Meridional): Un contacto mayor en la cadena Hercínica Europea, Ph.D. Thesis, Univ. de Granada, 327 pp., 1991.

Crouzet, C., Dunkl, I., Paudel, L., Arkai, P., Rainer, T.M., Balogh, K., and Appel, E.: Temperature and age constraints on the metamorphism of the Tethyan Himalaya in Central Nepal: A multidisciplinary approach, Journal of Asian Earth Sciences, 30(1), 113-130, 2007.

Dahn, D.R.L., Braid, J.A., Murphy, J.B., Quesada, C., Dupuis, N., and McFarlane C.R.M.: Geochemistry of the Peramora Melange and Pulo do Lobo schist: Geochemical investigation and tectonic interpretation of mafic melange in the Pangean suture zone, Southern Iberia, International Journal of Earth Sciences, 103(5), 1415-1431, 2014.

Dallmeyer, R.D., Fonseca, P.E., Quesada, C., and Ribeiro, A.: $^{40}Ar/^{39}Ar$ mineral age constraints for the tectonothermal evolution of a variscan suture in Southwest Iberia, Tectonophysics, 222, 177-194, 1993.

De Andrade, V., Vidal, O., Lewin, E., O'Brien, P., and Agard, P.: Quantification of electron microprobe compositional maps of rock thin sections: an optimized method and examples, Journal of Metamorphic Geology, 24(7), 655-668, 2006.

Díaz Azpiroz, M., Fernández, C., Castro, A., and El-Biad, M.: Tectonometamorphic evolution of the Aracena metamorphic belt (SW Spain) resulting from ridge-trench interaction during Variscan plate convergence, Tectonics, 25(1), 2006.

Eden, C.P.: Tectonostratigraphic analysis of the northern extent of the oceanic exotic terrane, Northwestern Huelva Province, Spain, Ph. D. Thesis, Univ. of Southampton, 214 pp., 1991.

Eden, C., and Andrews, J.: Middle to upper Devonian melanges in SW Spain and their relationship to the Meneage formation in south Cornwall. Proc. Ussher Soc., 7, 217-222, 1990.

Endo, S., and Wallis, S.R.: Structural architecture and low-grade metamorphism of the Mikabu-Northern Chichibu accretionary wedge, SW Japan, Journal of Metamorphic Geology, 35(6), 695-716, 2017.

Ernst, W.G.: Tectonic history of subduction zones inferred from retrograde blueschist PT paths, Geology 16(12), 1081-1084, 1988.

Ernst, W.G.: Alpine and Pacific styles of Phanerozoic mountain building: subduction-zone petrogenesis of continental crust, Terra Nova, 17(2), 165-188, 2005.

Escuder Viruete, J., Arenas, R., and Martínez Catalán, J.R.: Tectonothermal evolution associated with Variscan crustal extension in the Tormes gneiss dome (NW Salamanca, Iberian Massif, Spain), Tectonophysics, 238(1-4), 117-138, 1994.

871 Fonseca, P., and Ribeiro, A.: Tectonics of the Beja-Acebuches ophiolite - a major suture in the Iberian
872 variscan foldbelt, Geol. Rundsch., 82, 440-447, 1993.

873 Fonseca, P., Munhá, J., Pedro, J., Rosas, F., Moita, P., Araujo, A., and Leal, N.: Variscan ophiolites
874 and high-pressure metamorphism in southern Iberia. Ofioliti, 24, 259-268, 1999.

875 Franceschelli, M., Leoni, L., Memmi, I., and Puxeddu, M.: Regional distribution of Al-silicates and
876 metamorphic zonation in the low-grade Verrucano metasediments from the Northern
877 Apennines, Italy, Journal of Metamorphic Geology, 4(3), 309-321, 1986.

878 Frey, M.: Very low-grade metamorphism of clastic sedimentary rocks, in: Low temperature
879 metamorphism, edited by: Frey, M., Blackie, Glasgow, 9-58, 1987.

880 Frey, M., and Robinson, D.: Low-Grade Metamorphism, 313 pp. Blackwell Science Ltd, Cambridge,
881 1999.

882 Gil Ibarguchi, J., Mendia, M., Girardeau, J., and Peucat, J.J.: Petrology of eclogites and clinopyroxene-
883 garnet metabasites from the Cabo Ortegal Complex (northwestern Spain), Lithos, 25(1-3),
884 133-162, 1990.

885 Goffé, B., and Velde, B.: Contrasted metamorphic evolutions in thrusted cover units of the
886 Briançonnais zone (French Alps): A model for the conservation of HP-LT metamorphic
887 mineral assemblages, Earth and Planetary Science Letters, 68(2), 351-360, 1984.

888 Grosch, E.G., Vidal, O., Abu-Alam, T., and McLoughlin, N.: P–T constraints on the metamorphic
889 evolution of the Paleoarchean Kromberg type-section, Barberton greenstone belt, South
890 Africa, Journal of Petrology, 53(3), 513-545, 2012.

891 Grosch, E.G., McLoughlin, N., Lanari, P., Erambert, M., and Vidal, O.: Microscale mapping of
892 alteration conditions and potential biosignatures in basaltic-ultramafic rocks on early Earth
893 and beyond, Astrobiology, 14(3), 216-228, 2014.

894 Guidotti, C.V., and Sassi, F.P.: Classification and correlation of metamorphic facies series by means
895 of muscovite b data from low-grade metapelites, Neues Jahrbuch fur Mineralogie-
896 Abhandlungen, 153, 363-380, 1986.

897 Guidotti, C. V., Mazzoli, C., Sassi, F. P., and Blencoe, J. G.: Compositional controls on the cell
898 dimensions of 2M 1 muscovite and paragonite, European Journal of Mineralogy, 4(2), 283-
899 297, 1992.

900 Guidotti, C.V., Sassi, F.P., Blencoe, J.G., and Selverstone, J.: The paragonite–muscovite solvus: I. P-
901 T-X limits derived from the Na – K compositions of natural, quasibinary paragonite-
902 muscovite pairs, Geoch. Cosmochim. Acta, 58, 2269–2275, 1994.

903 Gutiérrez-Alonso, G., and Nieto, F.: White-mica 'crystallinity', finite strain and cleavage development
904 across a large Variscan structure, NW Spain, Journal of the Geological Society, 153(2), 287-
905 299, 1996.

906 Hilchie, L.J., and Jamieson, R.A.: Graphite thermometry in a low-pressure contact aureole, Halifax,
907 Nova Scotia, Lithos, 208, 21-33, 2014.

908 Jarosewich, E.J., Nelen, J.A., and Norberg, J.A.: Reference samples for electron microprobe analysis:
909 Geostandards Newsletter, 4, 43-47, 1980.

910 Kisch, H.J.: Correlation between indicators of very low-grade metamorphism. In: Low temperature
911 metamorphism, edited by: Frey, M., Blackie, Glasgow, 227-300, 1987.

912 Kisch, H.J.: Illite crystallinity: recommendations on sample preparation, X-ray diffraction settings,
913 and interlaboratory samples, Journal of Metamorphic Geology, 9, 665–670, 1991.

914 Kübler, B. : Evaluation quantitative du metamorphism par la cristallinite de l'Illite. Bull. Centres Rech.
915 Pau-SNPA 2, 385-397, 1968.

916 Lahfid, A., Beyssac, O., Deville, E., Negro, F., Chopin, C., and Goffé, B.: Evolution of the Raman
917 spectrum of carbonaceous material in low-grade metasediments of the Glarus Alps
918 (Switzerland), Terra Nova, 22, 354-360, 2010.

919 Lanari, P., Guillot, S., Schwartz, S., Vidal, O., Tricart, P., Riel, N., and Beyssac, O. : Diachronous
920 evolution of the alpine continental subduction wedge: evidence from P-T estimates in the
921 Briançonnais Zone houillère (France-Western Alps), Journal of Geodynamics, 56-57, 39-54,
922 2012.

923 Lanari, P., Vidal, O., de Andrade, V., Dubacq, B., Lewin, E., Grosch, E.G., and Schwartz, S.:
924 XMapTools: A MATLAB©-based program for electron microprobe X-Ray image
925 processing and geothermobarometry, Computers & Geosciences, 62, 227-240, 2014a.

926 Lanari, P., Rolland, Y., Schwartz, S., Vidal, O., Guillot, S., Tricart, P., and Dumont, T.: P–T–t
927 estimation of deformation in low-grade quartz-feldspar-bearing rocks using thermodynamic
928 modelling and 40Ar/39Ar dating techniques: example of the Plan-de-Phasy shear zone unit
929 (Briançonnais Zone, Western Alps), Terra Nova, 26(2), 130-138, 2014b.

930 Lopes, G., Pereira, Z., Fernandes, P., Wicander, R., Matos, J.X., Rosa, D., and Oliveira, J.T.: The
931 significance of reworked palynomorphs (middle Cambrian to Tournaisian) in the Visean
932 Toca da Moura Complex (South Portugal). Implications for the geodynamic evolution of
933 Ossa Morena Zone, Rev. Palaeobot. Palynol., 200, 1-23, 2014.

934 López-Carmona, A., Pitra, P., and Abati, J.: Blueschist-facies metapelites from the Malpica-Tui Unit
935 (NW Iberian Massif): phase equilibria modelling and H2O and Fe2O3 influence in high-
936 pressure assemblages, Journal of Metamorphic Geology, 31(3), 263-280, 2013.

937 López Munguira, A., Nieto, F., Pardo, E. S., and Velilla, N.: The composition of phyllosilicates in
938 Precambrian, low-grade metamorphic, clastic rocks from the Southern Hesperian Massif
939 (Spain) used as an indicator to metamorphic conditions, Precambrian Research, 53(3-4), 267-
940 279, 1991.

941 López Sánchez-Vizcaíno, V., Gómez Pugnaire, M.T., Azor, A., and Fernández Soler, J.M.: Phase
942 diagram sections applied to amphibolites: a case study from the Ossa-Morena/Central
943 Iberian Variscan suture (Southwestern Iberian Massif), Lithos, 68, 1-21, 2003.

944 Martínez Catalán, J.R.: Estratigrafia y estructura del Domo de Lugo (Sector Oeste de la Zona
945 Asturoccidental-leonesa), Corpus Geol. Gallaeacie (2º Serie), 2, 1-291, 1985.

946 Martínez Catalán, J.R., Rubio Pascual, F.J., Díez Montes, A., Díez Fernández, R., Gómez Barreiro,
947 J., Dias Da Silva, Í., González Clavijo, E., Ayarza, P., and Alcock, J.E.: The late Variscan
948 HT/LP metamorphic event in NW and Central Iberia: relationships to crustal thickening,
949 extension, orocline development and crustal evolution, Geological Society, London, Special
950 Publications, 405(1), 225-247, 2014.

951 Martínez Poyatos, D., Nieto, F., Azor, A., and Simancas, J.F.: Relationships between very low-grade
952 metamorphism and tectonic deformation: Examples from the southern Central Iberian Zone
953 (Iberian Massif, Variscan Belt), Journal of the Geological Society, 158, 953-968, 2001.

954 Martínez Poza, A.I., Martínez Poyatos, D., Simancas, J.F., and Azor, A.: La estructura varisca de la
955 Unidad del Pulo do Lobo (SO del Macizo Ibérico) en las transversales de Aroche y Rosal de
956 la Frontera (Huelva), Geogaceta, 52, 21-24, 2012.

957 Massonne, H.J., and Schreyer, W.: Phengite geobarometry based on the limiting assemblage with K-
958 feldespar, phlogopite, and quartz, Contributions to Mineralogy and Petrology, 96, 212-224,
959 1987.

960 Massonne, H.J., and Szpurka, Z.: Thermodynamic properties of white micas on the basis of high-
961 pressure experiments in the systems $K_2O$-MgO-$Al_2O_3$- $SiO_2$-$H_2O$ and $K_2O$-FeO-$Al_2O_3$-
962 $SiO_2$-$H_2O$. Lithos, 41, 229–250, 1997.

963 Matte, P.: The Variscan collage and orogeny (480-290 Ma) and the tectonic definition of the Armorica
964 microplate: A review, Terra Nova, 13, 122-128, 2001.

965 Merriman, R.J., and Frey, M.: Patterns of very low-grade metamorphism in metapelitic rocks, in: Low-
966 grade metamorphism, edited by: Frey, M., and Robinson, D., Blackwell, Oxford, 61–107,
967 1999.

968 Moita, P., Munhá, J., Fonseca, P., Pedro, J., Araújo, A., Tassinari, C., and Palacios, T.: Phase equilibria
969 and geochronology of Ossa-Morena eclogites, Actas do XIV Semana de Gequímica / VIII
970 Congresso de geoquímica dos Países de Língua Portuguesa, 2, 471-474, 2005.

971 Moore, D.M., and Reynolds, R.C. Jr.: X-ray Diffraction and the Identification and Analysis of Clay
972 Minerals, 2nd edition, Oxford University Press, Oxford, 1997.

973 Mori, H., Mori, N., Wallis, S., Westaway, R., and Annen, C.: The importance of heating duration for
974 Raman CM thermometry: evidence from contact metamorphism around the Great Whin Sill
975 intrusion, UK, Journal of Metamorphic Geology, 35(2), 165-180, 2017.

976 Munhá, J.: Metamorphic evolution of the south Portuguese/Pulo do Lobo zone, in: Pre-Mesozoic
977 Geology of Iberia, edited by: Dallmeyer, R.D., and Martínez García, E., Springer, Berlin,
978 Germany, pp. 363-368, 1990.

979 Murphy, J. B., Quesada, C., Gutiérrez-Alonso, G., Johnston, S. T. and Weil, A.: Reconciling
980 competing models for the tectono-stratigraphic zonation of the Variscan orogen in Western
981 Europe. Tectonophysics, 681, 209-219, 2016.

982 Nieto, F., and Sánchez-Navas, A.: A comparative XRD and TEM study of the physical meaning of
983 the white mica «crystallinity» index, European Journal of Mineralogy, 6(5), 611-621, 1994.

984 Nieto, F., Mata, M.P., Bauluz, B., Giorgetti, G., Árkai, P., and Peacor, D.R.: Retrograde diagenesis, a
985 widespread process on a regional scale, Clay Minerals, 40(1), 93-104, 2005.

986 Oliveira, J.T.: Part VI: South Portuguese Zone, stratigraphy and synsedimentary tectonism, in: Pre-
987 Mesozoic Geology of Iberia, edited by: Dallmeyer, R.D., and Martínez García, E., Springer,
988 Berlin, Germany, pp. 334-347, 1990

989 Olsson, I.: Regional burial heating vs. local magmatic heat influence of the Röstånga area, Scania,
990 southern Sweden, GFF, 121(3), 209-214, 1999.

991 Omrani, H., Moazzen, M., Oberhänsli, R., and Moslempour, M.E.: Iranshahr blueschist: subduction
992 of the inner Makran oceanic crust, Journal of Metamorphic Geology, 35(4), 373-392, 2017.

993 Ordóñez-Casado, B.: Geochronological studies of the Pre-Mesozoic basement of the Iberian Massif:
994 the Ossa-Morena Zone and the Allochthonous Complexes within the Central Iberian Zone,
995 Ph.D. Thesis, ETH Zurich, 235 pp., 1998.

Parra, T., Vidal, O., and Agard, P., A thermodynamic model for Fe-Mg dioctahedral K White micas using data from phase-equilibrium experiments and natural pelitic assemblages, Contrib. Mineral Petrol., 143, 706-732, 2002.

Pedro, J., Araujo, A., Fonseca, P., Tassinari, C., and Ribeiro, A.: Geochemistry and U-Pb Zircon Age of the Internal Ossa-Morena Zone Ophiolite Sequences: A Remnant of Rheic Ocean in SW Iberia, Ofioliti, 35(2), 117-130, 2010.

Pereira, M.F., Apraiz, A., Chichorro, M., Silva, J.B., and Armstrong, R.A.: Exhumation of high pressure rocks in northern Gondwana during the Early Carboniferous (Coimbra-Cordoba shear zone, SW Iberian Massif): tectonothermal analysis and U-Th-Pb SHRIMP in-situ zircon geochronology, Gondwana Research, 17, 440-460, 2010.

Pereira, M.F., Chichorro, M., Silva, J.B., Ordóñez-Casado, B., Lee, J.K., and Williams, I.S.: Early carboniferous wrenching, exhumation of high-grade metamorphic rocks and basin instability in SW Iberia: constraints derived from structural geology and U-Pb and $^{40}Ar$-$^{39}Ar$ geochronology, Tectonophysics, 558, 28-44, 2012.

Pereira, M.F., Chichorro, M., Williams, I.S., Silva, J.B., Fernández, C., Díaz-Azpíroz, M., Apraiz, A., and Castro, A.: Variscan intra-orogenic extensional tectonics in the Ossa-Morena Zone (Évora-Aracena-Lora del Río metamorphic belt, SW Iberian Massif): SHRIMP zircon U-Th-Pb geochronology, Geological Society, London, Special Publications, 327(1), 215-237, 2009.

Pereira, M.F., Martínez Poyatos, D., Pérez-Cáceres, I., Gama, C., and Azor, A.: Comment on "Stratigraphy of the Northern Pulo do Lobo Domain, SW Iberia Variscides: A palynological contribution" by Pereira, Z. et al. (2018) - Geobios, 51, 491-506. Geobios, in press, 2019.

Pereira, Z., Matos, J., Fernandes, P., and Oliveira, J.T.: Palynostratigraphy and systematic palynology of the Devonian and Carboniferous successions of the South Portuguese Zone, Portugal, Memórias Geológicas do Instituto Nacional de Engenharia, Tecnologia e Inovaçao 34, Lisboa, 2008.

Pereira, Z., Fernandes, P., Matos, J., Jorge, R., and Oliveira, J.T.: Stratigraphy of the Northern Pulo do Lobo Domain, SW Iberia Variscides: A palynological contribution, Geobios, 51, 491-506, 2018.

Pérez-Cáceres, I., Martínez Poyatos, D., Simancas, J.F., and Azor, A.: The elusive nature of the Rheic Ocean in SW Iberia, Tectonics, 34, 2429-2450, 2015.

Pérez-Cáceres, I., Simancas, J.F., Martínez Poyatos, D., and Azor, A.: Oblique collision and deformation partitioning in the SW Iberian Variscides, Solid Earth, 7, 857-872, 2016.

Pérez-Cáceres, I., Martínez Poyatos, D., Simancas, J.F., and Azor, A.: Testing the Avalonian affinity of the South Portuguese Zone and the Neoproterozoic evolution of SW Iberia through detrital zircon populations, Gondwana Research, 42, 177-192, 2017.

Pérez-Estaún, A., Bea, F. and Vera, J. A.: Macizo Ibérico, Edited by: Vera, J.A., Geología de España, 19-228, 2004.

Petschick R.: http://www.geol-pal.uni-frankfurt.de/Staff/Homepages/Petschick/classicsoftware.html# MacDiff, 2004.

Platt, J. P.: Dynamics of orogenic wedges and the uplift of high-pressure metamorphic rocks, Geological Society of America Bulletin, 97(9), 1037-1053, 1986.

Ponce, C., Simancas, J.F., Azor, A., Martínez Poyatos, D.J., Booth-Rea, G., and Expósito, I.: Metamorphism and kinematics of the early deformation in the Variscan suture of SW Iberia, Journal of Metamorphic Geology, 30(7), 625-638, 2012.

Potel, S., Ferreiro-Mählmann, R., Stern, W. B., Mullis, J., and Frey, M.: Very low-grade metamorphic evolution of pelitic rocks under high-pressure/low-temperature conditions, NW New Caledonia (SW Pacific), Journal of Petrology, 47(5), 991-1015, 2006

Potel, S., Maison, T., Maillet, M., Sarr, A. C., Doublier, M. P., Trullenque, G., and Mählmann, R. F.: Reliability of very low-grade metamorphic methods to decipher basin evolution: Case study from the Markstein basin (Southern Vosges, NE France), Applied Clay Science, 134, 175-185, 2016.

Quesada, C.: Precambrian successions in SW Iberia: their relationship to 'Cadomian'orogenic events. Geological Society, London, Special Publications, 51(1), 353-362, 1990.Quesada, C., Fonseca, P.E., Munhá, J., Oliveira, J.T., and Ribeiro, A.: The Beja-Acebuches Ophiolite (Southern Iberia Variscan fold belt): geological characterization and significance, Boletín Geológico Minero, 105, 3-49, 1994.

Quesada, C., Braid, J. A., Fernandes, P., Ferreira, P., Jorge, R. S., Matos, J. X., Murphy, J.B., Oliveira, J.T., Pedro, J. and Pereira, Z.: SW Iberia Variscan Suture Zone: Oceanic Affinity Units. In The Geology of Iberia: A Geodynamic Approach, Volume 2: The Variscan Cycle, edited by: Quesada, C., and Oliveira, J.T., Springer. 131-171. Springer, 2019.

Ribeiro, A., Munhá, J., Fonseca, P.E., Araujo, A., Pedro, J.C., Mateus, A., Tassinari, C., Machado, G., and Jesus, A.: Variscan ophiolite belts in the Ossa-Morena Zone (Southwest Iberia): Geological characterization and geodynamic significance, Gondwana Research, 17(2-3), 408-421, 2010.

Rubio Pascual, F.J., Matas J., and Martín Parra, L.M.: High-pressure metamorphism in the Early Variscan subduction complex of the SW Iberian Massif, Tectonophysics, 592, 187-199, 2013.

Sassi, F.P., and Scolari, A.: The $b_0$ value of the potassic white micas as a barometric indicator in low-grade metamorphism of pelitic schists, Contributions to Mineralogy and Petrology, 45(2), 143-152, 1974.

Silva, J. B., Oliveira, J.T., and Ribeiro, A.: South Portuguese Zone, structural outline, in: Pre-Mesozoic Geology of Iberia, edited by: Dallmeyer, R.D., and Martínez García, E., Springer, Berlin, Germany, pp. 348-362, 1990.

Simancas, J.F., Carbonell, R., Lodeiro, F.G., Pérez-Estaún, A., Juhlin, C., Ayarza, P., Kashubin, A., Azor, A., Martínez Poyatos, D., Almodóvar, G.R., Pascual, E., Sáez, R., and Expósito, I.: Crustal structure of the transpressional Variscan orogen of SW Iberia: SW Iberia deep seismic reflection profile (IBERSEIS), Tectonics, 22(6), 1062, 2003.

Simancas, J.F., Expósito, I., Azor, A., Martínez Poyatos, D., and González Lodeiro, F.: From the Cadomian orogenesis to the Early Palaeozoic Variscan rifting in Southwest Iberia, Journal of Iberian Geology, 30, 53-71, 2004.

Simancas, J.F., Carbonell, R., González Lodeiro, F., Pérez-Estaún, A., Juhlin, C., Ayarza, P., Kashubin, A., Azor A., Martínez Poyatos, D.J., Sáez, R., Almodóvar, G.R., Pascual R., Flecha, I., and Martí, D.: Transpressional collision tectonics and mantle plume dynamics: The Variscides of southwestern Iberia, Memoirs, Geol. Soc., 32(1), 345-354, 2006.

Vázquez, M., Abad, I., Jiménez-Millán, J., Rocha, F.T., Fonseca, P.E., and Chaminé, H.I.: Prograde epizonal clay mineral assemblages and retrograde alteration in tectonic basins controlled by major strike-slip zones (W Iberian Variscan chain), Clay Minerals, 42(1), 109-128, 2007.

Vidal, O., Parra, T., and Trotet, F.: A thermodynamic model for Fe-Mg aluminous chlorite using data from phase equilibrium experiments and natural pelitic assemblages in the 100-600 °C 1-25 kbar range, American Journal of Science, 63, 557-592, 2001.

1085 Vidal, O., Parra, T., and Vieillard, P.: Thermodynamic properties of the Tschermak solid solution in
1086 Fe-chlorite: application to natural examples and possible role of oxidation, American
1087 Mineralogist, 90, 347-358, 2005.

1088 Vidal, O., de Andrade, V., Lewin, E., Muñoz, M., Parra, T., and Pascarelli, S.: P-T-deformation-
1089 Fe3+/Fe2+ mapping at the thin section scale and comparison with XANES mapping.
1090 Application to a garnet-bearing metapelite from the Sambagawa metamorphic belt (Japan),
1091 Journal of Metamorphic Geology, 24, 669-683, 2006.

1092 Vidal, O., Lanari, P., Munoz, M., Bourdelle, F., and De Andrade, V.: Deciphering temperature,
1093 pressure and oxygen-activity conditions of chlorite formation, Clay Minerals, 51(4), 615-633,
1094 2016.

1095 Warr, L.N., and Ferreiro Mählmann, R.: Recommendations for Kübler Index standardization, Clay
1096 Minerals, 50(3), 283-286, 2015.

1097 Warr, L.N., and Rice, A.H.N.: Inter-laboratory standardization and calibration of clay mineral
1098 crystallinity and crystallite size data, Journal of Metamorphic Geology, 12, 141–152, 1994.

1099 Whitney, D.L., and Evans, B.W.: Abbreviations for names of rock-forming minerals, American
1100 mineralogist, 95(1), 185, 2010.

Figure 1

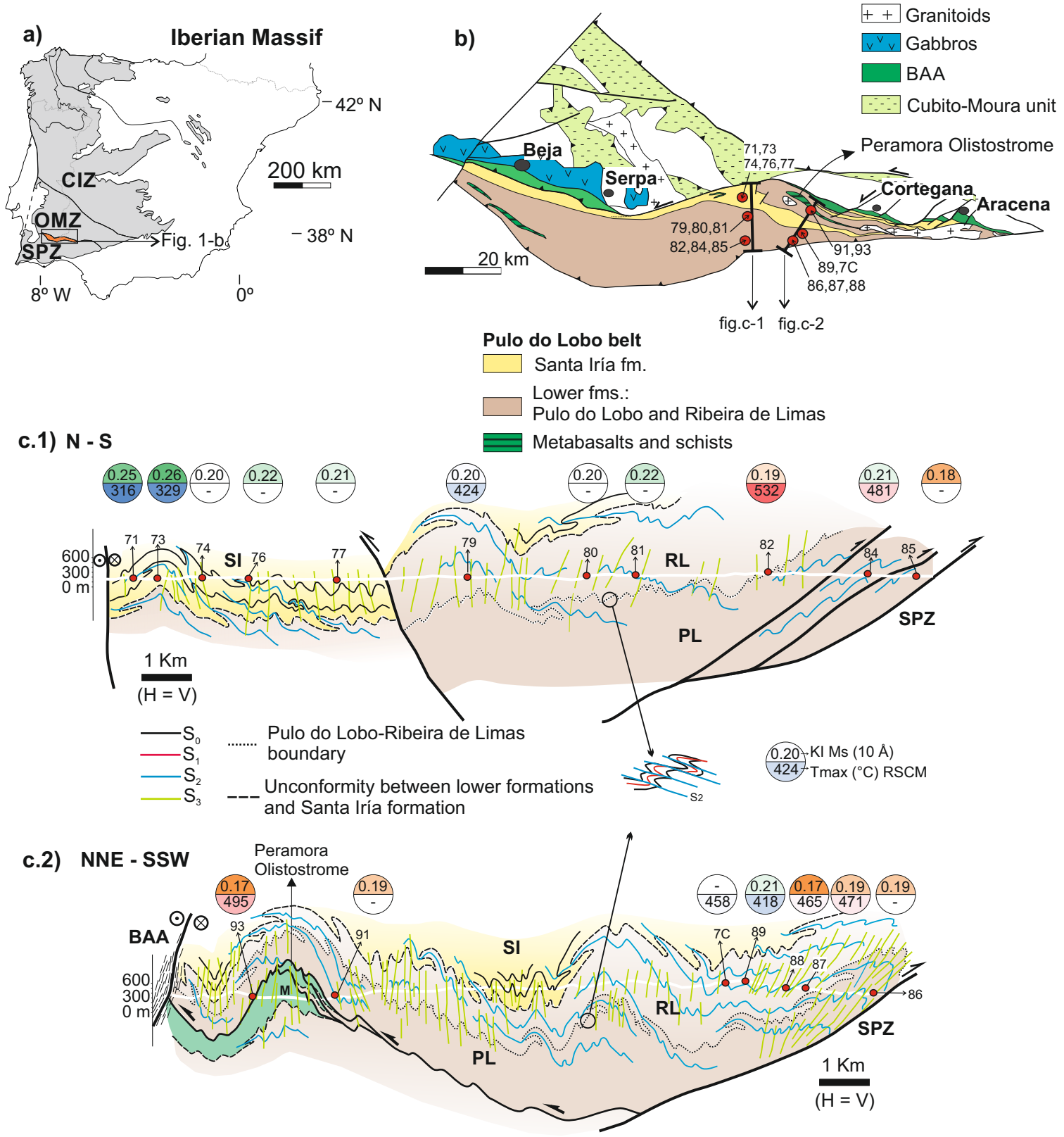
a)
Iberian Massif
42º N
200 km
38º N
CIZ
OMZ
SPZ
Fig. 1-b
8º W
0º
b)
Granitoids
Gabbros
BAA
Cubito-Moura unit
Peramora Olistostrome
Beja
Serpa
Cortegana
Aracena
71,73
74,76,77
79,80,81
82,84,85
91,93
89,7C
86,87,88
20 km
fig.c-1
fig.c-2
Pulo do Lobo belt
Santa Iría fm.
Lower fms.:
Pulo do Lobo and Ribeira de Limas
Metabasalts and schists
c.1) N - S
SI
RL
PL
SPZ
1 Km
(H = V)
S0
S1
S2
S3
Pulo do Lobo-Ribeira de Limas boundary
Unconformity between lower formations and Santa Iría formation
KI Ms (10 Å)
Tmax (°C) RSCM
c.2) NNE - SSW
Peramora Olistostrome
BAA
SI
RL
PL
SPZ
M
1 Km
(H = V)

Figure 2

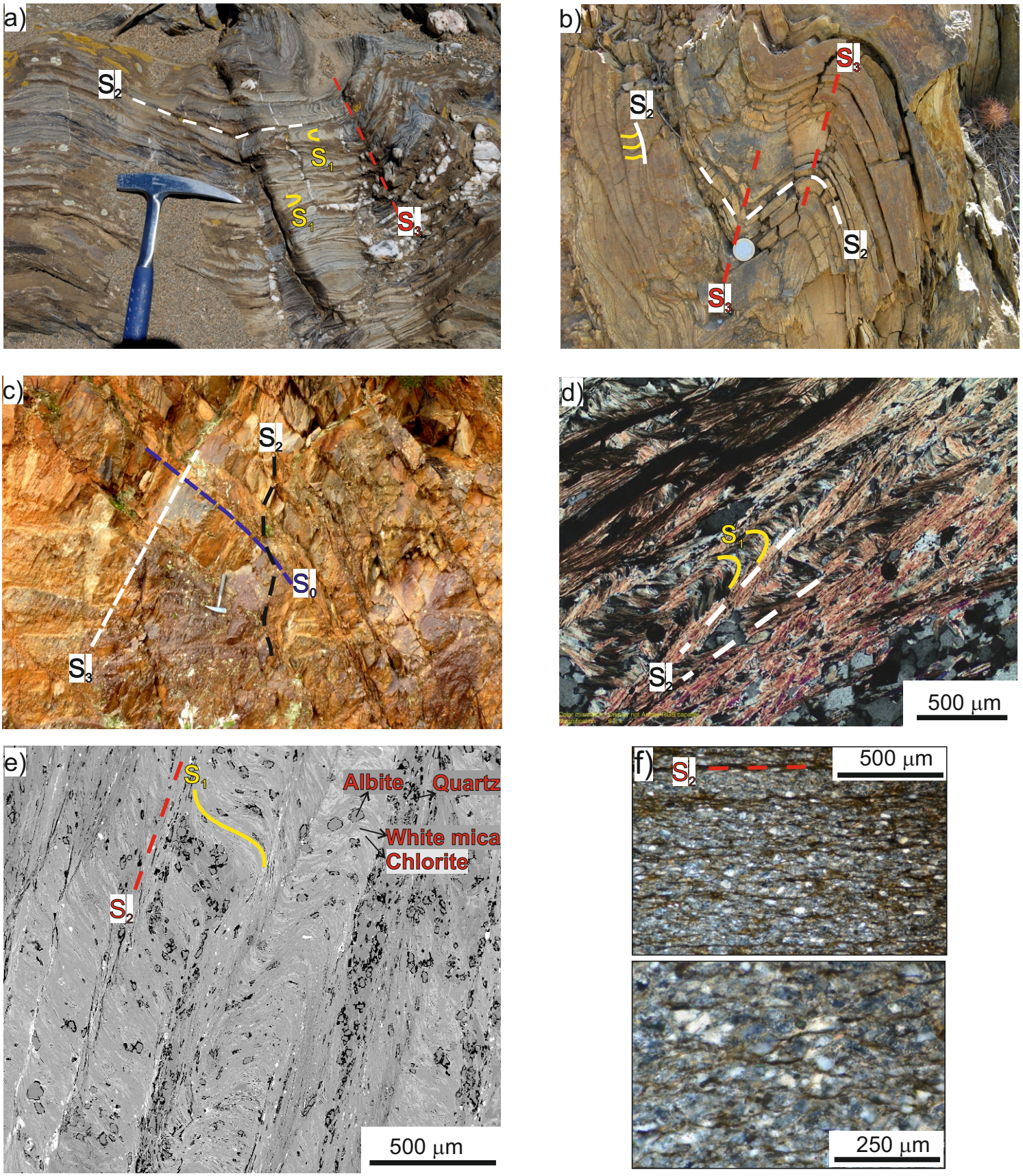
a)
$S_2$
$S_1$
$S_1$
$S_3$
b)
$S_3$
$S_2$
$S_2$
$S_3$
c)
$S_2$
$S_0$
$S_3$
d)
$S_1$
$S_2$
500 µm
e)
$S_1$
$S_2$
Albite
Quartz
White mica
Chlorite
500 µm
f)
$S_2$
500 µm
250 µm

Figure 3

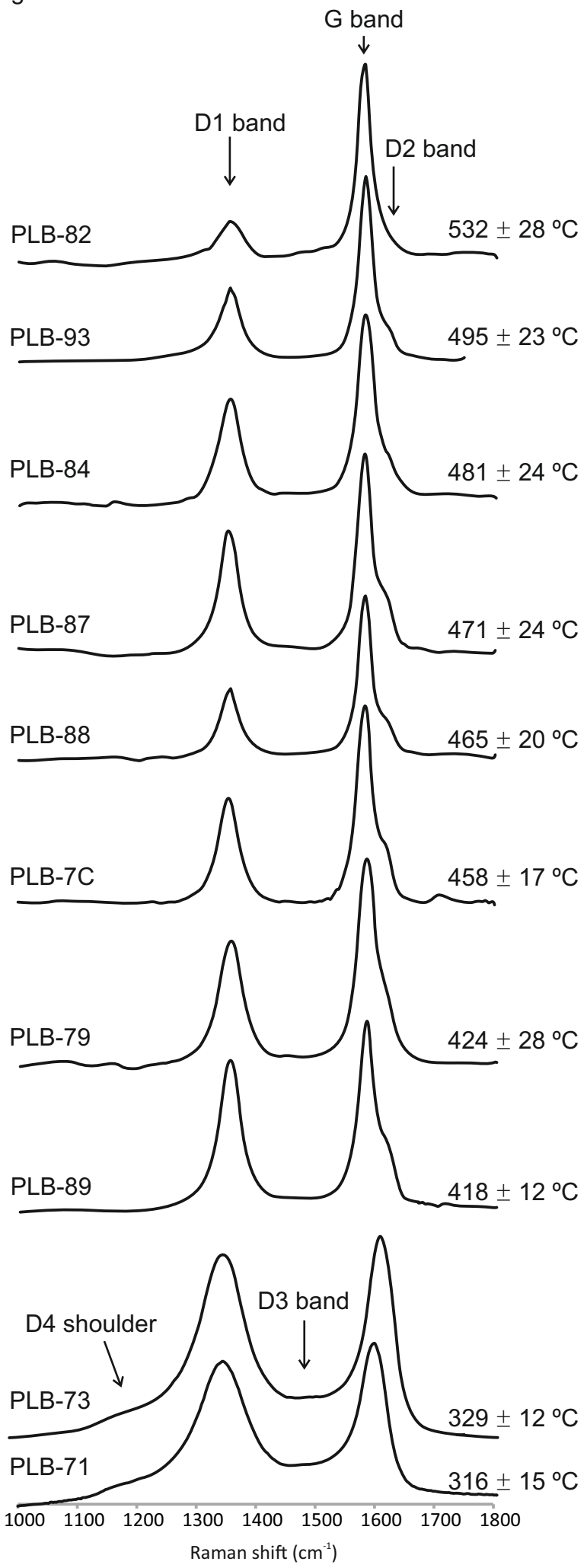
G band
D1 band
D2 band
PLB-82
532 ± 28 ºC
PLB-93
495 ± 23 ºC
PLB-84
481 ± 24 ºC
PLB-87
471 ± 24 ºC
PLB-88
465 ± 20 ºC
PLB-7C
458 ± 17 ºC
PLB-79
424 ± 28 ºC
PLB-89
418 ± 12 ºC
D4 shoulder
D3 band
PLB-73
329 ± 12 ºC
PLB-71
316 ± 15 ºC
1000 1100 1200 1300 1400 1500 1600 1700 1800
Raman shift (cm-1)

Figure 4

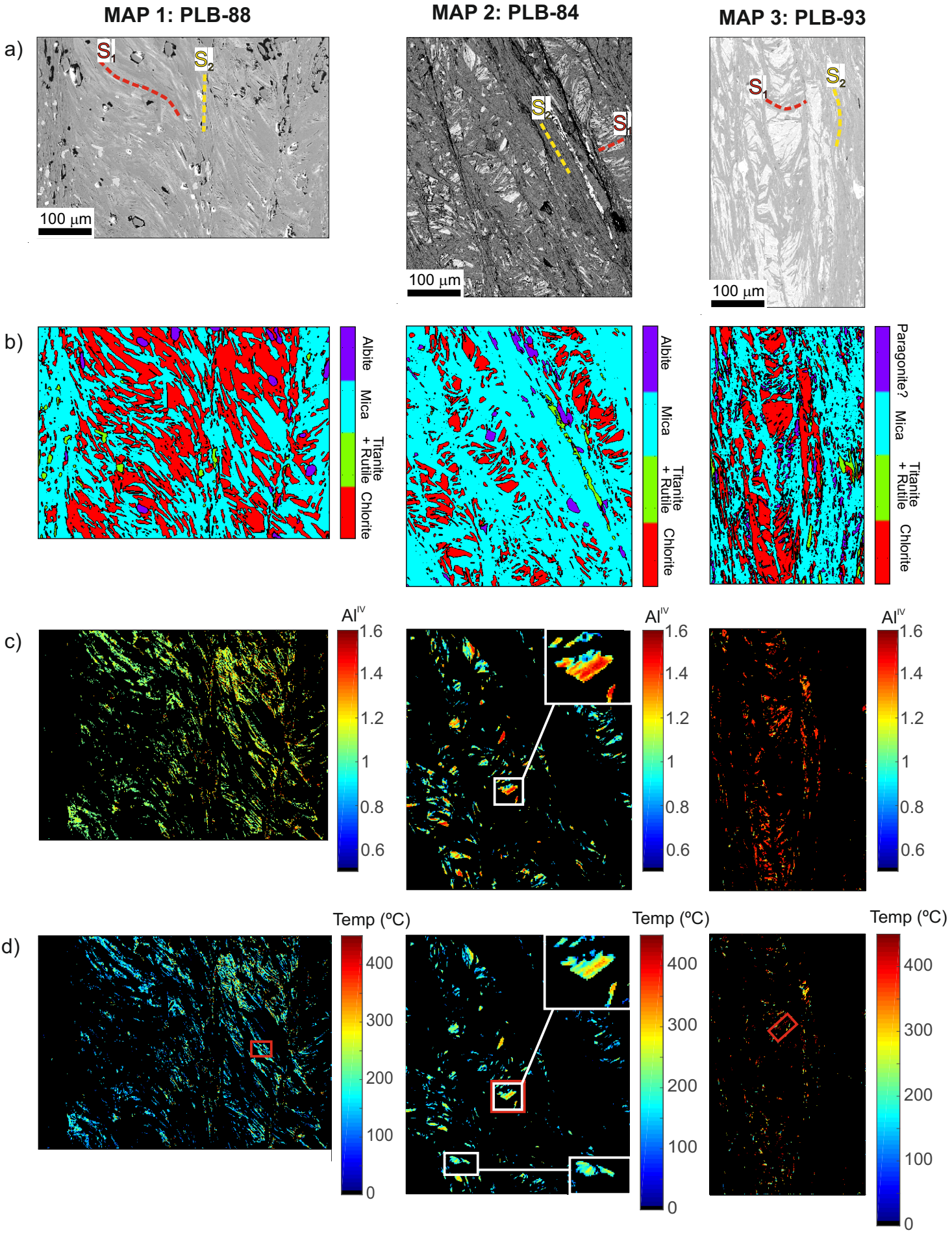
MAP 1: PLB-88
MAP 2: PLB-84
MAP 3: PLB-93
a)
S1
S2
100 µm
b)
Albite
Mica
Titanite + Rutile
Chlorite
Paragonite?
c)
AlIV
1.6
1.4
1.2
1
0.8
0.6
d)
Temp (ºC)
400
300
200
100
0

Figure 5

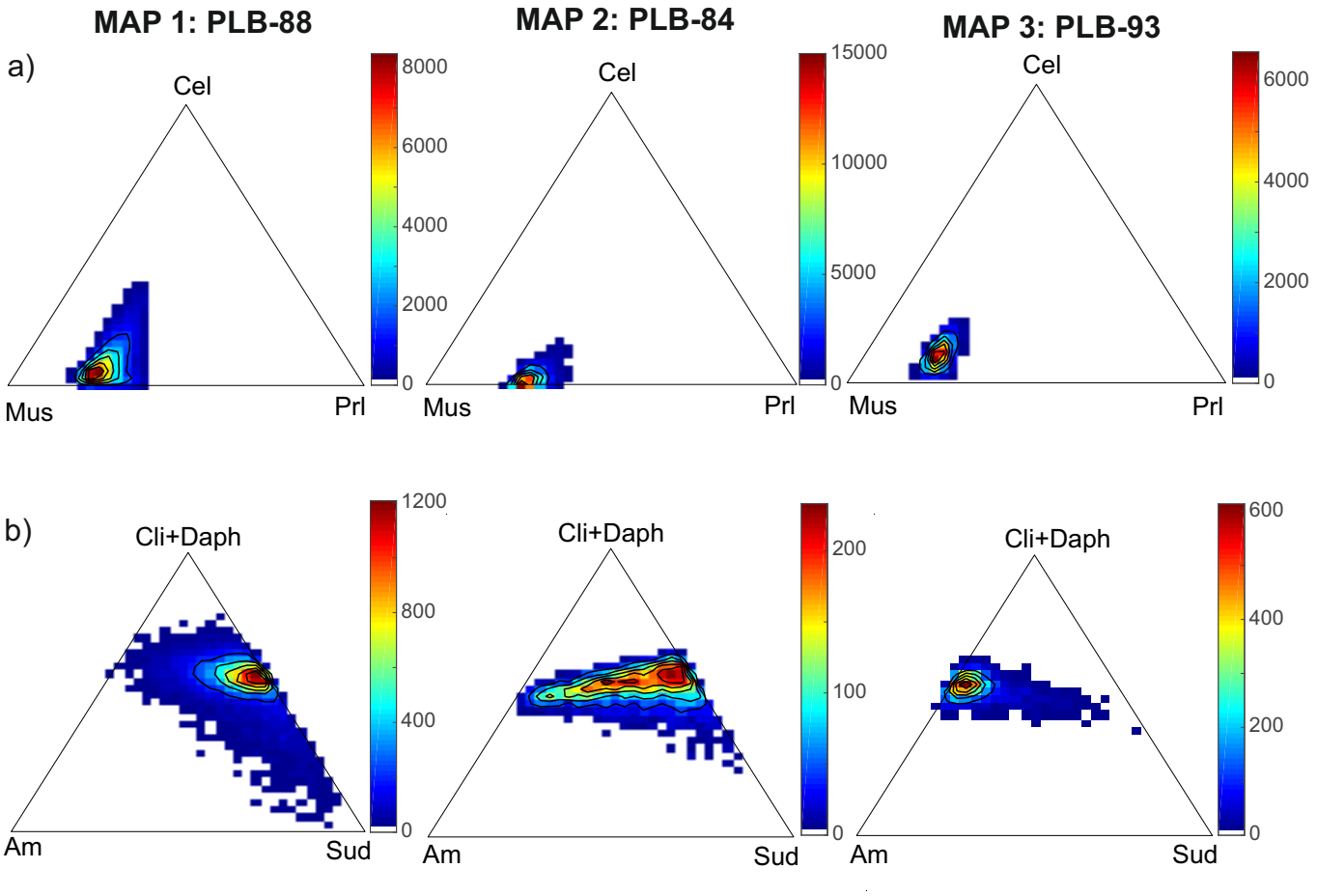
MAP 1: PLB-88
MAP 2: PLB-84
MAP 3: PLB-93
a)
Cel
Mus
Prl
8000
6000
4000
2000
0
15000
10000
5000
b)
Cli+Daph
Am
Sud
1200
800
400
200
100
600

Figure 6

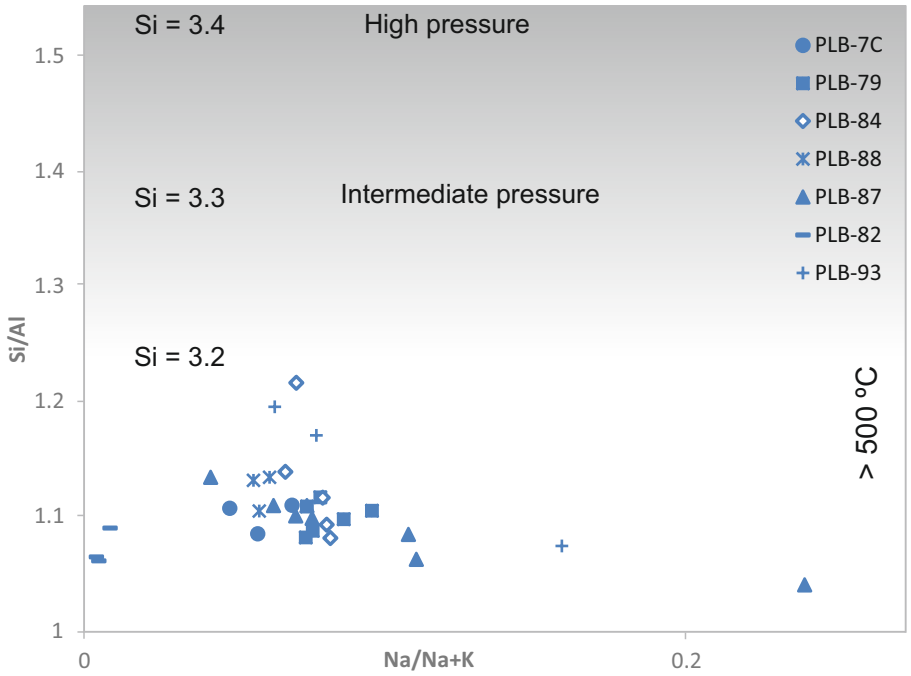
Si = 3.4
High pressure
Si = 3.3
Intermediate pressure
Si = 3.2
> 500 °C
PLB-7C
PLB-79
PLB-84
PLB-88
PLB-87
PLB-82
PLB-93
Si/Al
1.5
1.4
1.3
1.2
1.1
1
0
0.2
Na/Na+K

Figure 7

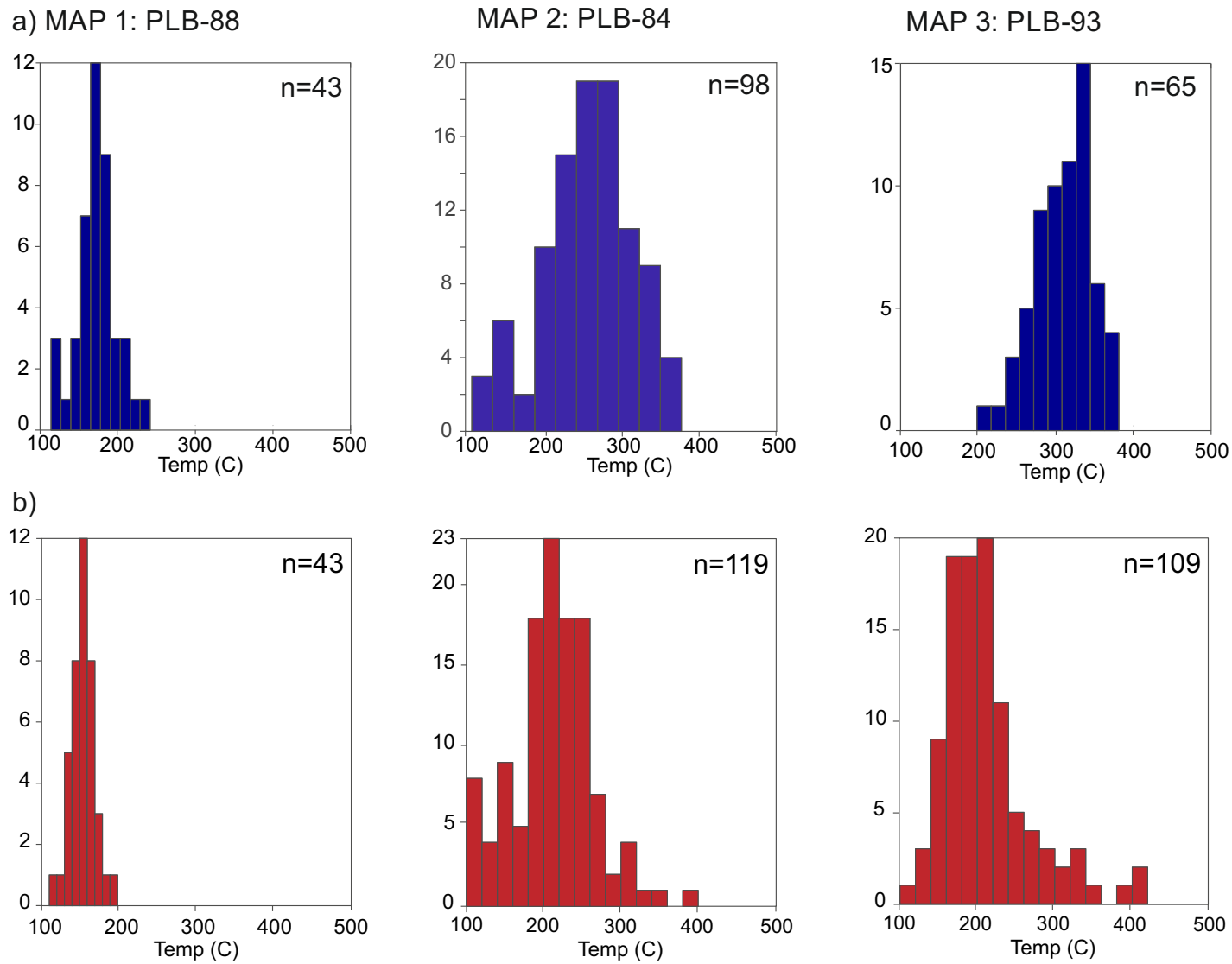
a) MAP 1: PLB-88
MAP 2: PLB-84
MAP 3: PLB-93
n=43
n=98
n=65
Temp (C)
b)
n=43
n=119
n=109
Temp (C)

**Table 1**

| Formation | Sample | Mineralogy | FWHM | Basel KI (10 Å) | | b (Å) | $d_{001}$ (Å) | White mica compositions | | | Chlorite compositions | | | Chlorite maps (Lanari et al., 2014b) | Chlorite thermometry | | $T_{max}$ (°C) RSCM | |
|---|---|---|---|---|---|---|---|---|---|---|---|---|---|---|---|---|---|---|
| | | | | | | | | | | | | | | | Vidal et al., 2006 | Bourdelle et al., 2013 | | |
| | PLB- | Qz + Ms + Fsp+ | Å | bulk fraction | <2 µm | Ms | Ms | % Ms | % Cel | % Prl | % Cli+Daph | % Am | % Sud | T (°C) | T (°C) | T (°C) | Mean | Std Dv |
| Santa Iría (upper formation) | 71 | Chl | 0.221 | 0.23 | 0.25 | 8.991 | 9.995 | - | | | - | | | - | - | - | 316 | 15 |
| | 73 | Chl | 0.227 | 0.22 | 0.26 | 8.996 | 9.997 | - | | | - | | | - | - | - | 329 | 12 |
| | 74 | Chl + C/S | 0.164 | 0.20 | 0.20 | 8.999 | 10.001 | - | | | - | | | - | - | - | - | |
| | 76 | Chl | 0.184 | 0.20 | 0.22 | 8.997 | 9.997 | - | | | - | | | - | - | - | - | |
| | 77 | Chl + C/S | 0.171 | 0.19 | 0.21 | 8.998 | 9.995 | - | | | - | | | - | - | - | - | |
| lower fomations | 79 | Chl + Pg | 0.17 | 0.18 | 0.20 | 8.995 | 9.993 | - | | | - | | | - | - | - | 424 | 28 |
| | 80 | Chl | 0.169 | 0.18 | 0.20 | 9.001 | 9.988 | - | | | - | | | - | - | - | - | |
| | 81 | Chl + Pg + C/S | 0.181 | 0.19 | 0.22 | - | 9.988 | - | | | - | | | - | - | - | - | |
| | 82 | Chl + Pg | 0.158 | 0.17 | 0.19 | 8.995 | 9.986 | - | | | - | | | - | - | - | 532 | 28 |
| | 84 (map 2) | Chl + Pg + C/S | 0.173 | 0.17 | 0.21 | 8.994 | 9.988 | 70-80 | 0-10 | 20-30 | 50 | 0-50 | 0-50 | 150-350 | 150-375 | 150-350 | 481 | 24 |
| | 85 | Chl + Pg | 0.137 | 0.17 | 0.18 | 8.996 | 9.996 | - | | | - | | | - | - | - | - | |
| | 86 | Pg + C/S | 0.144 | 0.18 | 0.19 | 8.993 | 9.986 | - | | | - | | | - | - | - | - | |
| | 87 | Chl + Pg | 0.144 | 0.18 | 0.19 | 8.998 | 9.986 | - | | | - | | | - | - | - | 471 | 24 |
| | 88 (map 1) | Chl + Pg | 0.129 | 0.18 | 0.17 | 8.997 | 9.990 | 70-80 | 0-10 | 20-30 | 50 | 0-10 | 20-50 | 100-200 | 120-230 | 150-200 | 465 | 20 |
| | 89 | Chl | 0.178 | 0.19 | 0.21 | 8.996 | 9.993 | - | | | - | | | - | - | - | 418 | 12 |
| | 91 | Chl + Pg | 0.143 | 0.17 | 0.19 | 9.000 | 9.995 | - | | | - | | | - | - | - | - | |
| | 93 (map 3) | Chl + Pg | 0.128 | 0.18 | 0.17 | 9.002 | 9.990 | 70-80 | 0-10 | 20-30 | 50 | 40-50 | 0-10 | 200-450 | 200-380 | 150-400 | 495 | 23 |
| | 7C | - | - | - | - | 8.993 | - | - | | | - | | | - | - | - | 458 | 17 |

**Table 2**

| Time | Deformation/metamorphic phase | Temperature | Low-grade metamorphic conditions |
|---|---|---|---|
| Middle-Upper Carboniferous | $S_3$<br>$S_2$-$M_2$ | -<br><300 °C | -<br>Epizone-Anchizone limit |
| Early Carboniferous<br>(~340 Ma) | Beja-Acebuches and Pulo do Lobo metamafics<br>Thermal imprint | | |
| Upper Devonian | $S_1$-$M_1$ | ~300-450 °C | Epizone |